Macromolecules

pubs.acs.org/Macromolecules Article

Synthesis of a Double-Hydrophilic Block Copolymer with a Multifunctional Block: Spontaneous Formation of Polyion Complex Micelles from a Single Cationic−Anionic Copolymer

Ananthapadmanabhan Unnikrishnan, Mateus Garcia Rodolfo, Najet Mahmoudi, Gaulthier Rydzek,* Julien Schmitt,* Ralf Schweins, and Corine Gérardin

Cite This: *Macromolecules* 2025, 58, 5110−5134 Read Online

ACCESS | Metrics & More | Article Recommendations | Supporting Information

ABSTRACT: A double-hydrophilic block copolymer (DHBC) exhibiting a multifunctional block was obtained via a multistep synthesis. First, the parent copolymer, Par. Pol., P(OEGMEA)-*b*-PAA, composed of a neutral block of poly(oligo(ethylene glycol))-methyl ether acrylate (P(OEGMEA)) and a weak polyacid block of poly(acrylic acid) (PAA), was synthesized by RAFT polymerization. Then, the PAA block was modified via the activation/amidation route, using *N*-(3-(dimethylamino)propyl)-*N*′-ethyl-carbodiimide (EDC) and *N*-hydroxysuccinimide (NHS) to activate the DHBC, yielding the activated copolymer Act. Pol., before reaction with *N*-Boc ethylenediamine. The resulting amidated copolymer, named Ami. Pol., composed of P(OEGMEA)-*b*-P(AA-*s*-(Acyl urea)-*s*-(N-Boc)), exhibits several functional groups on the second block: acrylates from the PAA backbone, pending *N*-Acyl urea, and finally pending *N*-Boc ethylenediamine. *N*-Acyl urea exhibits tertiary amines, while *N*-boc ethylenediamine adds primary amines protected by a *tert*-butyl group, which can later be removed by a deprotection step using trichloroacetic acid (TCA), yielding the final P(OEGMEA)-*b*-P(AA-*s*-(Acyl urea)-*s*-(AA/NH_2)) copolymer, labeled De. Pol. We characterized the DHBC at every stage of the modification (i.e., parent copolymer, activated copolymer, amidated copolymer, and deprotected copolymer) using a combination of NMR and elemental analysis to assess the number of units of each group in the second block. After activation/amidation, *N*-Acyl urea groups represent ca. 13−32% of the second block, depending on the activation conditions, while the amount of *N*-Boc ethylenediamine groups is ca. 8−34%, depending on the amidation conditions. We demonstrated the efficient removal of the *tert*-butyl protection groups after deprotection without any damage to the DHBC. Due to the presence of acrylates and amine functions, the activated, amidated, and deprotected copolymers exhibit pH-tunable self-assembling properties. Samples were studied at pH values ranging from 2 to 9, using dynamic light scattering (DLS), ζ-potential measurements, and ATR-FTIR, and well-defined micelles were observed at pH values ranging from 4−9. The combination of measurements, coupled with DLS studies as a function of salt, provided evidence that micelles were formed by electrostatic complexation between the positively charged *N*-Acyl urea pending groups and the unmodified negatively charged acrylate species. Micelles were then characterized using a combination of light and small-angle neutron scattering (SANS). Notably, an optimum pH range for micellization of 5−7 with a single population was obtained by dynamic light scattering (DLS). SANS data were successfully fitted using a model of polymer micelles, which provided information about the core radius of the micelles R (6.3 ± 0.1 nm for amidated copolymer at pH = 5), the gyration radius of the P(OEGMEA) chains in the micelle shell R_g (3.3 ± 0.1 nm), and the polydispersity in size σ (13 ± 1%). SANS patterns of amidated copolymers as a function of concentration were also studied, and data were successfully fitted by adding a hard-sphere structure factor, providing evidence of intermicellar interactions. Finally, SANS patterns of the deprotected copolymer showed a decrease in the core radius (R = 5.3 ± 0.1 nm at pH = 5), consistent with the removal of the bulky *tert*-butyl groups. The method developed here allows the formation of DHBCs that not only exhibit self-assembling properties in water due to the addition of *N*-Acyl urea groups but also present extra functional groups (in our case, primary amines).

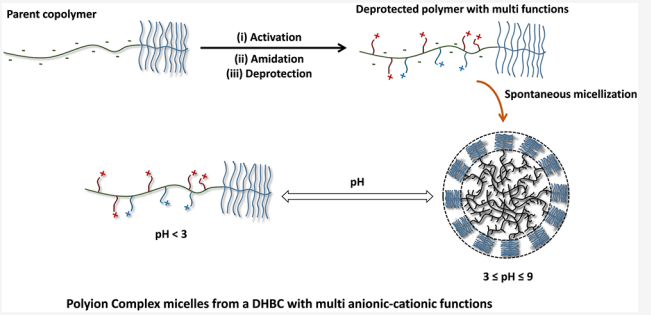

1. INTRODUCTION

Block copolymers, composed of well-defined blocks of different chemical natures, have attracted particular attention as structuring agents for self-assembled nanomaterials.[1−3] Many of them display amphiphilic behavior due to differences in the hydrophilicity of the copolymer blocks. Finely

Received: November 21, 2024
Revised: March 17, 2025
Accepted: April 4, 2025
Published: May 5, 2025

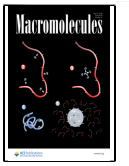

https://doi.org/10.1021/acs.macromol.4c02884
Macromolecules 2025, 58, 5110−5134

Scheme 1. Methodology to Design a DHBC, Which Exhibits Self-Assembling Properties in Water While Presenting Several Functions on its Second Block[a]

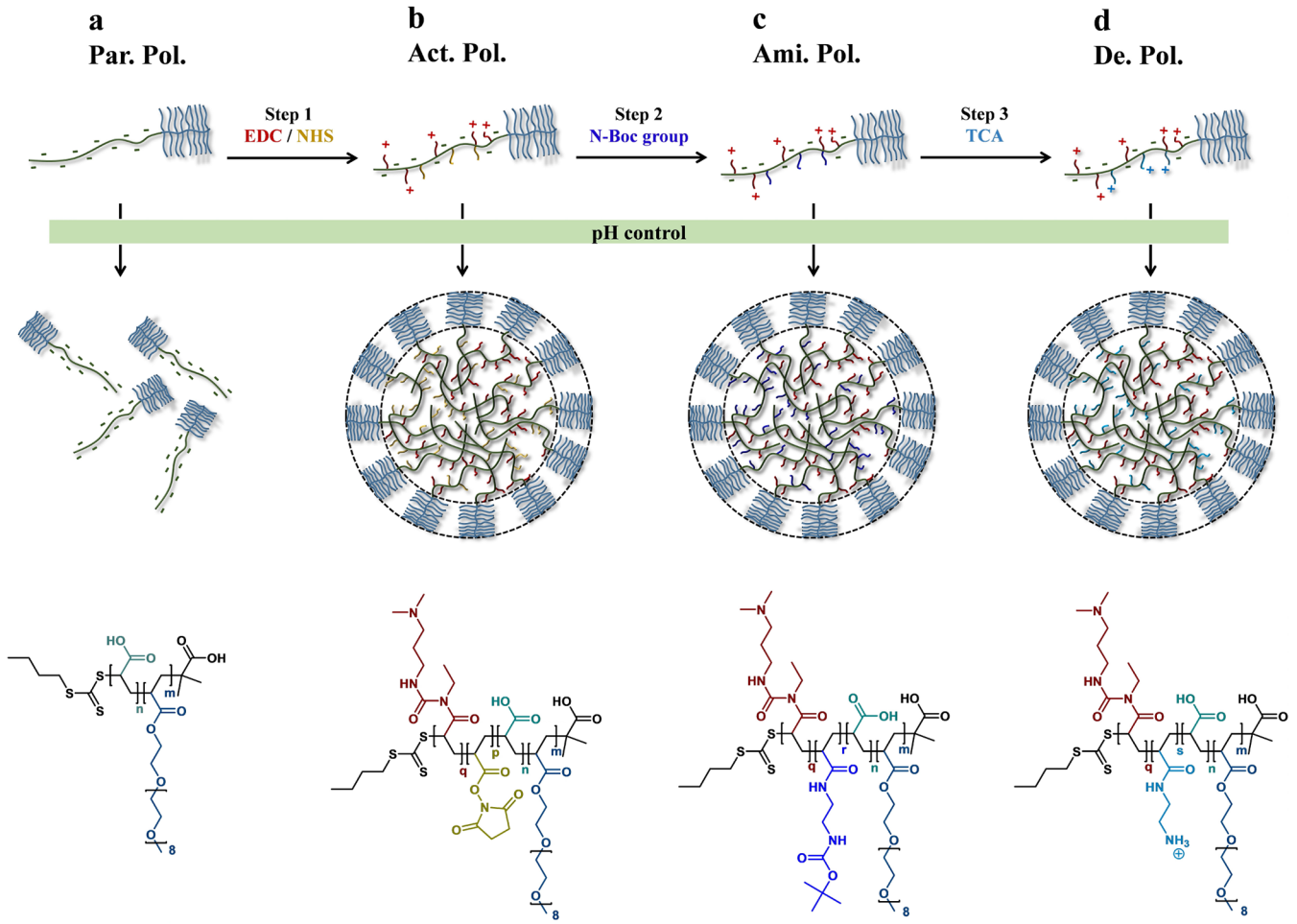

[a]Step 1: Activation of a previously synthesized P(OEGMEA)-*b*-P(AA) parent polymer (Par. Pol.) (a) with EDC/NHS forms an activated copolymer (Act. Pol.) made of P(OEGMEA)-*b*-P(AA-*s*-(AA-NHS)-*s*-(Acyl urea)) (b). Step 2: Amidation of Act. Pol. by reaction with *N*-Boc-ethylenediamine forms an amidated polymer (Ami. Pol.) made of P(OEGMEA)-*b*-P(AA-*s*-(Acyl urea)-*s*-(*N*-Boc)) (c). Step 3: Deprotection by reaction with TCA removes the *tert*-butyl group of the *N*-Boc-ethylenediamine, freeing the primary amine functions of the final deprotected polymer (De. Pol.), P(OEGMEA)-*b*-P(AA-*s*-(Acyl urea)-*s*-(AA/NH_2)) DHBC (d). The P(OEGMEA) comb-like block is shown in classic blue, the PAA linear block in green, NHS-activated esters in yellow, *N*-Acyl urea pendant functions in red, the protected amine in navy blue, and the primary amine functions in turquoise. At the bottom of the scheme, the chemical structure of each DHBC is given.

controlling the chemical structure and relative mass fraction of each block allows these copolymers to spontaneously self-assemble in aqueous solutions to form micelles, fibers, vesicles, and microphase-separated matrices.[4−6] A specific type of block copolymer, the double hydrophilic block copolymer (DHBC), is distinguished by its entirely hydrophilic nature, but some of them can still micellize in aqueous solvents under specific conditions.[7,8] Indeed, DHBCs can self-assemble in water in response to internal or external stimuli, such as pH,[9,10] ionic strength,[9,11] temperature,[10,11] or the nature of added solvents,[12] which selectively decrease the hydrophilicity of one of the blocks and trigger the self-assembly, while the second block remains hydrophilic and ensures the formation of stable core−shell micelles. Thanks to a judicious choice of the two blocks of the DHBC, researchers have been able to form pH-sensitive vesicles (using zwitterionic polymers)[13] or even structure-reversible micelles, whose core and shell can be switched using a DHBC with dual thermosensitivity.[14] This has paved the way for multi-stimuli-responsive DHBCs,[15−17] with applications as drug carriers that often require controlled breaking of the carrier at a specific pH or temperature,[18−20] or as catalytic nanoreactors, where micellization enhances the catalytic properties of the polymer.[21]

Some DHBCs, exhibiting a charged block and a neutral block, require a micellization partner to form micelles in solution via electrostatic interaction between the charged block of the DHBC and a micellization partner of opposite charge. Depending on the type of micellization partner, polyelectrolyte or multivalent metal ion, the micelles formed are labeled as polyion complex (PIC)[22−24] or hybrid polyion complex (HPIC)[25,26] micelles, respectively. HPIC micelles have found a natural application in the field of nanoparticle synthesis by using the micelle core as a nanoreactor for particle growth (with the metal ions as precursors), while the shell of the micelles controls the size of the nanoparticles and the overall shape of the micelles, influencing that of the nanoparticles.[27−31] PIC (and HPIC) micelles have also found a fascinating application in the formation of mesoporous

https://doi.org/10.1021/acs.macromol.4c02884
Macromolecules 2025, 58, 5110−5134

functional materials.[32−36] An example lies in DHBCs comprising a neutral ethylene oxide-based hydrophilic block (for instance, poly(oligo(ethylene glycol) methyl ether acrylate) P(OEGMEA)) and a polyelectrolyte block (for instance, poly(acrylic acid) P(AA)). PIC micelles formed with these DHBCs can be used as both structure-directing and functionalizing agents for the formation of an ordered mesoporous structure whose pores are functionalized by polyelectrolytes.[37] These dual features are related to the specific properties of the two blocks of the DHBC: the ethylene oxide units of the neutral block strongly interact with silicic species in aqueous solution via hydrogen bonding to form the hybrid interface of the material, while the polyelectrolyte block imparts its functionality to the final material.[32,33] In the case of weak polyelectrolytes, the pH-dependent ionization rate of the charged block of the DHBC and of the micellization partner controls the range of pH associated to (H)PIC micelles formation. This mechanism places requirements on the micellization partner, such as good coacervation properties, but also on the formulation, including the fine control of the ratio of micellization partner to DHBC in solution, a controlled pH window, and the efficient removal of the micellization partner after material formation. Further, a salient limitation of this approach is that the nature of the polyelectrolyte block of the DHBC chosen must be adapted each time to the targeted application; this implies designing new polymer synthesis procedures for each new DHBC. Since direct polymerization with target functions is not always easily achievable, this methodological drawback limits the variety of functions that can be integrated into PIC micelles and their resulting functional hybrid materials. Hence, it prevents versatile use of the functional materials. Thus, our goal is to design a P(OEGMEA)-based DHBC whose polyelectrolyte block exhibits several complementary functional groups in order to provide both direct self-assembly properties in aqueous solution and versatility in targeted applications.

This goal can be achieved by postsynthesis modification of the DHBC in order to specifically tune the physicochemical properties of its polyelectrolyte block without degrading its neutral block.[38−40] For instance, introducing specific hydrophilic and hydrophobic sections within the copolymer allows its self-assembly under aqueous conditions.[23,24,41,42] Postsynthesis modification also enables the addition of functional groups that are not easily accessible through direct polymerization.[38] In the case of acrylic and methacrylic polymers, a common method is to activate carboxylic acids using *N*-hydroxysuccinimide (NHS)[43−45] to form active esters that enhance their amidation reaction with nucleophilic amine species under mild aqueous conditions, due to the stability of NHS-activated esters against hydrolysis.[38,46] NHS activation is typically achieved by using *N*-(3-(dimethylamino)propyl)-*N*′-ethylcarbodiimide (EDC), which increases the reactivity of carboxylic acids with NHS.[43−45] Examples of nucleophilic amines used for this amidation procedure include aliphatic and cycloaliphatic amines for therapeutic applications[47] while ethylenediamine provides access to pendant primary amines, unlocking applications ranging from CO_2 capture[48] to the removal of metallic pollutants.[49,50] In the latter case, the homobifunctional nature of ethylenediamine poses the challenge of cross-linking the polymer chains. It is therefore worth replacing it with *N*-Boc-ethylenediamine, where one of the amines is protected by the Boc-($(CH_3)_3COCO$) group, which can be removed at a later stage to free the primary amine.[51−54]

Here, postsynthesis modification has been developed as a novel and effective approach to form poly(acrylic acid)-based DHBCs that exhibit self-assembly capabilities with pH-sensitive micellization behavior, while containing additional functional primary amine pendant groups. We followed a multi-step strategy that is summarized in Scheme 1. First, the polyacid block of the parent P(OEGMEA)-*b*-P(AA)[35,55,56] copolymer, named Par. Pol. (a in Scheme 1) was activated via the EDC/NHS route in an aqueous medium. We demonstrated that the reaction of EDC with carboxylic acids also introduces *N*-Acyl urea pendant groups into the polymer, resulting in the activated copolymer, or Act. Pol. (b), composed of P(OEGMEA)-*b*-P(AA-*s*-(AA-NHS)-*s*-(Acyl urea)), with *AA-NHS* corresponding to 2,5-dioxopyrrolidin-1-yl acrylate species from the grafting of NHS to the backbone and Acyl urea to *N*-((3-(dimethylamino)propyl)carbamoyl)-*N*-ethylacrylamide groups formed by the reaction of EDC with acrylates.[57−59] The introduced *N*-Acyl urea groups contain a tertiary amine with a pK_{aH} of 9.76, which can provide positive charges to the modified polymer under mild pH conditions.[60,61] Meanwhile, NHS-activated esters are also formed on the PAA block and can further react by amidation with *N*-Boc-ethylenediamine. After this amidation step, the resulting amidated copolymer was named Ami. Pol. (c), composed of P(OEGMEA)-*b*-P(AA-*s*-(Acyl urea)-*s*-(N-Boc)), with *N*-Boc corresponding to *tert*-butyl (2-acrylamidoethyl)carbamate groups in the polymer. This copolymer was found to not only self-assemble in aqueous solutions as a result of the new interactions between acrylates from the PAA backbone and tertiary amines from grafted *N*-Acyl urea, but also to contain additional protected primary amines. Finally, a simple deprotection step allows the primary amines to be exposed, resulting in the deprotected copolymer, or De. Pol. (d), composed of P(OEGMEA)-*b*-P(AA-*s*-(Acyl urea)-*s*-(AA/NH_2)), where AA/NH_2 are *N*-(2-aminoethyl)acrylamide groups obtained after removal of the *tert*-butyl group.[51−54] The self-assembling behavior observed for the amidated copolymer is maintained after deprotection, while the primary amine groups can act as extra functional groups. Each DHBC modification step was characterized by nuclear magnetic resonance (NMR) and elemental analysis, while self-assembly properties were assessed by light scattering. The shape of the micelles was fully characterized using small-angle neutron scattering (SANS). Finally, the mechanisms of micellization were studied using ζ-potential measurements and ATR-FTIR as a function of pH, and by DLS as a function of salt concentration. This new DHBC has great potential for the direct formation of multifunctional mesoporous materials whose properties can be adjusted as a function of pH, depending on the need to expose the initial acrylic acid function or the new primary or tertiary amine functions obtained after modifications in the mesopores.

2. MATERIALS AND METHODS

2.1. Chemicals Used. Oligo(ethylene glycol) methyl ether acrylate (OEGMEA, 99%, M_n = 480 g/mol, 9 EO units on average) and acrylic acid (AA, 99%, M_n = 72.06 g/mol) were purchased from Sigma-Aldrich. Removal of radical inhibitors by adsorption with alumina particles (Sigma-Aldrich) was carried out prior to their use in polymerization. The initiator, 4,4′-azobis(4-cyanopentanoic acid) (ACPA, 98%) was pur-

https://doi.org/10.1021/acs.macromol.4c02884
Macromolecules 2025, 58, 5110−5134

chased from Sigma-Aldrich, while the chain transfer agent, 2-(butylthiocarbonothioylthio)-2-methylpropanoic acid (BDMAT), was synthesized according to previously documented protocols.[62,63] *N*-(3-Dimethylaminopropyl)-*N*′-ethylcarbodiimide (EDC, 98%) was purchased from Alfa Aesar and used as received. Meanwhile, *N*-hydroxysuccinimide (NHS, 98%) and *N*-Boc-ethylenediamine (≥98%) were also purchased from Sigma-Aldrich. Milli-Q water with a resistivity of 18.2 MΩ·cm at 25 °C was used for chemical synthesis and sample preparation. pH modification was carried out using NaOH and HCl (1 M and 5 M, respectively) solutions. For small-angle neutron scattering and NMR analysis, D_2O from Sigma-Aldrich was used as solvent.

2.2. P(OEGMEA)-*b*-P(AA) Synthesis. The parent copolymer, poly((oligoethylene glycol) methyl ether acrylate)-*b*-poly(acrylic acid), or P(OEGMEA)-*b*-P(AA), was synthesized using reversible addition−fragmentation chain-transfer polymerization (RAFT) in an aqueous solvent.[64] The synthesis of $P(OEGMEA)_{24}$-*b*-$P(AA)_{53}$ (35 wt % polymeric solution) was carried out as described below: BDMAT (0.1705 g, 7×10^{-4} mol) acting as the chain transfer agent, ACPA (0.0186 g, 7×10^{-5} mol) acting as the radical initiator, OEGMEA (7.59 g, 1.6×10^{-2} mol) monomer, and 14.4 mL of Milli-Q water were added to a 250 mL round-bottom flask. The reaction medium was stirred at ca. 250 rpm and purged with nitrogen for 30 min, followed by heating at 80 °C for 4.5 h. Subsequently, the second block was obtained by adding ACPA (0.0178 g, 6×10^{-5} mol), AA (2.40 g, 3.3×10^{-2} mol) and 4.5 mL of Milli-Q water to the reaction medium at room temperature. The reaction medium was then degassed again with nitrogen for 30 min, followed by heating at 80 °C under stirring. A 1 mL portion of the samples was collected after the synthesis of each block of the DHBC for ^{1}H NMR and elemental analysis. The degree of polymerization of each block, provided in Table 1, was determined from the ^{1}H NMR data as described in the Supporting Information. The sample is labelled Par. Pol. for parent polymer.

Table 1. Description of Parent Polymer (Par. Pol.) Obtained by RAFT Polymerization, with (For Each Block) the Degree of Polymerization (DP) Extracted from the Analysis of the NMR Spectra Given in Figure S1

Sample name	Type of polymer	DP P(OEGMEA)	DP P(AA)
Par.Pol.	P(OEGMEA)-*b*-P(AA)	24	53

2.3. Amidation of the Copolymer. Amidation of Par. Pol. (P(OEGMEA)-*b*-P(AA)) was carried out using EDC/NHS carboxylic acid activation, followed by an amidation reaction with N-Boc-ethylenediamine. We carried out six syntheses: one involving solely the activation step, yielding the activated copolymer Act. Pol., and five involving both the activation and amidation procedures, with variations in reaction time and pH, yielding the 5 amidated polymers, Ami. Pol. 1−5. The six polymers and their synthesis conditions are given in Table 2. Ami. Pol. 5 was synthesized for complementary measurements and was characterized only by NMR.

A typical amidation procedure, corresponding to P-$(OEGMEA)_{24}$-*b*-P$((AA)_{28}$-*s*-(Acyl urea)$_{17}$-*s*-(N-Boc)$_8$) (Ami. Pol. 1 in Table 2), is described as follows: P(OEGMEA)-*b*-P(AA) (2.55 g of 35 wt % Par. Pol. solution, 6×10^{-5} mol) was mixed in 10.0 mL of Milli-Q water in a 250 mL round-bottom flask and stirred at 200 rpm (temp: 50 °C) for 15 min. Then, EDC (0.823 g, 5×10^{-3} mol) diluted to 30 wt % (using 1.92 mL Milli-Q water) was added. Five minutes later, NHS (0.610 g, 5×10^{-3} mol) at 30 wt % (using 1.42 mL Milli-Q water) was introduced. After a certain activation time t_{act} (overnight for Ami. Pol. 1, 15 min for the others), a 30 wt % aqueous solution of *N*-Boc-ethylenediamine (0.832 g, 5×10^{-3} mol) was added to the reaction medium, which was left at 50 °C for >2 days to obtain the final amidated copolymer. The pH of all solutions except *N*-Boc-ethylenediamine (DHBC, EDC, NHS) was adjusted to pH_{act} (with pH_{act} = 7 for Ami. Pol. 1 and 2) using 1 M HCl or 1 M NaOH beforehand. Furthermore, after the addition of the *N*-Boc-ethylenediamine solution without pH regulation, the pH of the total reaction medium was adjusted to pH_{amid} (=8 for Ami. Pol. 1). After synthesis, the amidated copolymer Ami. Pol., P(OEGMEA)-*b*-P(AA-*s*-(Acyl urea)-*s*-(*N*-Boc)), was dialyzed against Milli-Q water for 3 days (with six solvent exchanges) using a dialysis bag with a molar mass cutoff of 2.5 kDa (from CelluSep membranes). It is worth noting that in the case of Act. Pol., the dialysis was carried out for 1 day only (involving two water exchanges) to try to avoid the removal of activated ester groups. Finally, the sample was freeze-dried.

Each sample was characterized by NMR and elemental analysis to calculate the number of units for each group and, hence, determine its precise chemical structure.

2.4. Deprotection of the Amidated Copolymer. Deprotection of amidated copolymer Ami. Pol. (P(OEGMEA)-*b*-P(AA-*s*-(Acyl urea)-*s*-(*N*-Boc))) was undertaken using trichloroacetic acid (TCA). In a 50 mL beaker, a ca. 1 wt % solution of Ami. Pol. was prepared in 10 mL of Milli-Q water, and the solution was stirred at room temperature for 1 h after the pH was adjusted to 1.75 using a 1 M TCA aqueous solution. After deprotection, the sample was purified by dialysis with Milli-Q water for 1 day (two water exchanges) using a cellulose dialysis bag with a molar mass cutoff of 2.5 kDa. Eventually, the sample was freeze-dried to obtain the final deprotected copolymer, De. Pol., with a chemical composition of P(OEGMEA)-*b*-P(AA-*s*-(Acyl urea)-*s*-(AA/NH_2)). The deprotection rate was evaluated by NMR and elemental analysis. Table 3 provides a list of deprotected samples prepared.

2.5. Preparation of Suspensions. Polymers (Par. Pol., Act. Pol., Ami. Pol. 1−5, or De. Pol. 1−4) were dispersed in aqueous suspensions for DLS/SLS or SANS analysis. Suspensions were prepared at room temperature. For DLS/SLS analysis, H_2O was used as the solvent, while D_2O was used for SANS. In light scattering experiments, samples were prepared at a concentration of 0.1 wt % in DHBC, while in neutron scattering, the typical concentration used was 1 wt %, unless stated otherwise. Similarly, for ζ-potential measurements made at various pH, samples were prepared at 1 wt %.

Regarding Act. Pol., suspensions for DLS/SLS and SANS were prepared at three different pH levels: 3, 5, and 9, to demonstrate the formation of micelles at pH = 5 and the effect of acidic (pH 3) or basic (pH 9) conditions on these micelles.

For the amidated polymers, several suspensions were prepared. For Ami. Pol. 1, the first samples were prepared again at pH = 5, and then a complete study of the role of pH was conducted by varying the pH between 2 and 9 in increments of 1. Similarly, for the same polymer, the role of concentration was studied using SANS at pH = 5 by examining concentrations ranging from 1 to 5 wt % in DHBC in

https://doi.org/10.1021/acs.macromol.4c02884
Macromolecules 2025, 58, 5110−5134

Table 2. List of Activated (Act. Pol.) and Amidated (Ami. Pol.) Polymers Prepared, along with Their Experimental Conditions and the Key Results Obtained from NMR and Elemental Analysis (EA)[a,b,c,d]

sample name	Block copolymer modified (number of units from NMR)	pH_{act}	pH_{amid}	*N*-Acyl urea Percentage	*N*-Boc amidation Percentage	Atomic ratio from EA N/C	Atomic ratio from EA S/C	Atomic ratio from EA H/C	Ratio calculated from NMR N/C	Ratio calculated from NMR S/C	Ratio calculated from NMR H/C
Act. Pol	$P(OEGMEA)_{24}$-*b*-$P((AA)_{25}$-*s*-$(AA\text{-}NHS)_{17}$-*s*-$(Acyl\ urea)_{11})$[e]	7	---	21	---	0.111	0.00119	2.25	0.111	0.000294	1.80
Ami .Pol. 1	$P(OEGMEA)_{24}$-*b*-$P((AA)_{28}$-*s*-$(Acyl\ urea)_{17}$-*s*-$(N\text{-}Boc)_8)$[f]	7	8	32	15	0.132	0.00010	2.28	0.102	0.000307	1.87
Ami. Pol. 2	$P(OEGMEA)_{24}$-*b*-$P((AA)_{28}$-*s*-$(Acyl\ urea)_{17}$-*s*-$(N\text{-}Boc)_8)$	7	8	32	15	0.130	0.00123	1.99	0.102	0.000307	1.87
Ami. Pol. 3	$P(OEGMEA)_{24}$-*b*-$P((AA)_{28}$-*s*-$(Acyl\ urea)_{23}$-*s*-$(N\text{-}Boc)_{18})$	9	9	23	34	0.110	0.00010	2.21	0.119	0.000282	1.88
Ami. Pol. 4	$P(OEGMEA)_{24}$-*b*-$P((AA)_{32}$-*s*-$(Acyl\ urea)_7$-*s*-$(N\text{-}Boc)_{14})$	8	8	13	26	0.111	0.00067	2.01	0.101	0.000304	1.87
Ami. Pol. 5	$P(OEGMEA)_{24}$-*b*-$P((AA)_{32}$-*s*-$(Acyl\ urea)_{17}$-*s*-$(N\text{-}Boc)_4)$	7	7	32	08	---	---	---	---	---	---

[a]Excess ratios used were ca. 1.70 for EDC, NHS, and *N*-Boc. The reaction time was 60 h in all cases except for Ami. Pol. 1, in which the reaction time was 84 h. [b]The pH conditions for both activation (pH_{act}) and amidation (pH_{amid}) are provided. [c]For all samples, the number of units of each block was obtained by NMR. This allowed estimating the percentage of activation and amidation obtained ($^{N}/_{N_{AA}}\cdot 100$) with *N*, the number of *N*-Acyl urea or *N*-Boc pending groups, and N_{AA}, the number of acrylates in Par. Pol.). [d]The number of units also allowed calculating the elemental atomic ratios N/C, S/C, and H/C, which were compared to the ratios found by EA. [e]The number of units were found using EA. [f]Activation time t_{act} = 16 h for this sample (vs 15 min for all the other Ami. Pol. samples).

Table 3. List of Deprotected Copolymers Prepared (De. Pol. 1 to 4)[a]

Sample name	Amidated copolymer used	Amidated copolymer used (DPs from NMR)	Deprotection: acid used, reaction time	Atomic ratio from EA N/C	Atomic ratio from EA S/C	Atomic ratio from EA H/C
De. Pol. 1	Ami. Pol. 1	$P(OEGMEA)_{24}$-*b*-$P((AA)_{28}$-*s*-$(Acyl\ urea)_{17}$-*s*-$(N\text{-}Boc)_8)$	TCA, 1Hour	0.115	0.00052	2.11
De. Pol. 2	Ami. Pol. 2	$P(OEGMEA)_{24}$-*b*-$P((AA)_{28}$-*s*-$(Acyl\ urea)_{17}$-*s*-$(N\text{-}Boc)_8)$	TCA, 1Hour	0.114	0.00078	2.07
De. Pol. 3	Ami. Pol. 3	$P(OEGMEA)_{24}$-*b*-$P((AA)_{28}$-*s*-$(Acyl\ urea)_{17}$-*s*-$(N\text{-}Boc)_8)$	TCA, 1day	0.119	0.00043	2.05
De. Pol. 4	Ami. Pol. 4	$P(OEGMEA)_{24}$-*b*-$P((AA)_{28}$-*s*-$(Acyl\ urea)_{17}$-*s*-$(N\text{-}Boc)_8)$	HCl, 1day	0.116	0.00095	2.04

[a]For each sample is given the amidated polymer (Ami. Pol.) used for deprotection, the conditions of deprotection (acid used and reaction time), the number of units of each block from NMR and the atomic ratios N/C, S/C, and H/C obtained by elemental analysis (EA).

increments of 1 wt %. To compare the different amidated polymers, Ami. Pol. 2 to 4 were also prepared at 1 wt % and pH = 5 for SANS studies. As Ami. Pol. 1−4 were used entirely in DLS and SANS, complementary ζ-potential measurements were carried out on a fifth sample, Ami. Pol. 5, at 1 wt % and pH ranging from 2 to 9. Finally, the effect of salt was studied in DLS on suspensions of Ami. Pol. 5 at 0.1 wt % and pH 5 by adding NaCl in order to achieve concentrations of 0, 0.1, 0.5, and 1 M.

Concerning the deprotected polymers, De. Pol. 1 was studied using both DLS/SLS and SANS at three pH levels (3, 5, and 9) to compare the results with the activated and amidated copolymers.

Lastly, the parent polymer Par. Pol. was also briefly studied at pH = 5 in DLS to confirm that micelles are not formed prior to DHBC modification. This sample was dispersed in 0.1 M NaCl to prevent electrostatic repulsion between PAA blocks.

Samples were prepared by mixing the required amount of DHBC with the solvent, followed by pH adjustment through the addition of HCl or NaOH (1 or 5 M, respectively).

2.6. Characterization Techniques. *2.6.1. NMR Spectroscopy.* ^{1}H NMR spectra of the copolymers were collected using a Bruker Avance III 600 MHz NMR Spectrometer using D_2O as the solvent. Regarding the parent copolymer, samples collected during polymerization were dried in an oven at 50 °C overnight, and approximately 10 mg were dissolved in 1 mL D_2O for characterization. Other samples (activated, amidated, and deprotected copolymers) were not directly dried to avoid unwanted reactions but were characterized by NMR after dialysis at neutral pH, freeze-drying and redispersion in D_2O (ca. 10 mg in 1 mL D_2O). The NMR data were processed using TopSpin 4.1.4, and chemical shifts (δ) are presented in ppm.

NMR data analysis allows for the extraction of the number of units of each pending group on the polymers. For Act. Pol., Ami. Pol., and De. Pol., conversion rates in *N*-Acyl urea and *N*-Boc pending groups correspond to the number of units of said group *N*, divided by N_{AA} = 53, the overall number of acrylate units in the parent polymer (see Table 2).

2.6.2. ATR-FTIR Spectroscopy. Attenuated total reflectance Fourier-transform infrared spectroscopy (ATR-FTIR) was performed in the 4000−400 cm^{-1} region using a Thermo Scientific Nicolet 4700 apparatus (USA) with a 0.5 cm^{-1} scan resolution. Act. Pol. and Ami. Pol. 1 were freeze-dried following the same procedure as for NMR analysis. For the studies as a function of pH, suspensions at 1 wt % of Ami. Pol. 5 at pH values ranging from 2 to 9 were prepared and homogenized before freeze-drying. To determine the ionization coefficient of the poly(acrylic acid) block for each pH, the carbonyl region of each spectrum was investigated extensively. The spectra were normalized using their most intense vibrational band (C−O stretching at ca. 1050 cm^{-1}) and the

https://doi.org/10.1021/acs.macromol.4c02884
Macromolecules 2025, 58, 5110−5134

region from 1350 to 1800 cm^{-1} was isolated. The Origin software was used to convert the transmittance spectra into absorbance, define their baseline, and subtract it. The carbonyl region (e.g., 1500 to 1800 cm^{-1}) exhibited 3 broads peaks that were deconvoluted using 5 gaussians corresponding to the carbonyl stretching in esters (1730 cm^{-1}), carboxylic acids (ca. 1700 cm^{-1}), amides (1640−1650 cm^{-1}), bound carboxylic acids (1620 cm^{-1}), and carboxylates (1560 cm^{-1}) as well as N−H bending from amides (1560 cm^{-1}).[65−67] An example of peak deconvolution is provided in Supporting Information. The positions and areas of the components corresponding to the ester and amide carbonyl bands were determined from the spectrum acquired at pH 9 and set as constraints for fitting the spectra at other pH values. No constraint was set for the other components during peak fitting. Due to the overlap of carboxylates and N−H bending bands, these two species were fitted within the same Gaussian component. At pH 2, that band almost disappeared, and its area was attributed to N−H bending only. This allowed for a minor correction to the peak areas measured at higher pH values, providing access to the contribution of carboxylate species. The ionization coefficient was determined using the following equation, where the factor 1.8 accounts for the different molar extinction coefficients of carboxylic acid and carboxylate species:[66]

$$\alpha = A(COO^-)/[A(COO^-) + 1.8.(A(COOH) + A(COOH)_{Bound})] \quad (1)$$

with $A(COO^-)$, $A(COOH)$ and $A(COOH)_{Bound}$ the peak areas related to the carboxylates, carboxylic acids and bound carboxylic acids stretching bands.

2.6.3. Elemental Analysis. Atomic percentages of C, H, N, and S in the dried samples were obtained via elemental analysis (approximately 50 mg of sample used for measurement) using a Thermo Fisher Scientific spectrometer iCE 3000. The drying procedure was the same as that used for NMR analysis.

2.6.4. ζ-Potential Measurements. The ζ-potential of Ami. Pol. 5 at 1 wt % and at pH ranging from 2−9 was measured using an AMERIGO system from Cordouan Technologies, France. All measurements were taken at room temperature. Laser Doppler electrophoresis measurements were performed using a laser at 638 nm and a 20.27 $V{\cdot}cm^{-1}$ applied electric field. The ζ-potentials were extracted from the electrophoretic mobility using the Smoluchowski equation. Results are presented as the average of 6 experiments along with their standard deviations.

2.6.5. Small-Angle Neutron Scattering (SANS). All samples were dispersed in D_2O and studied in 2 mm thick quartz cuvettes. The signal of D_2O alone was always recorded first. Concentrations between 1 and 5 wt % were used for the concentration studies, while the pH dependence of the samples was confirmed using 1 wt % solutions with a pH range from 2 to 9. A pH meter calibrated using H_2O was used to measure the samples. The pH of the micellar solution in D_2O can be obtained using the expression pD = 0.929 × pH* + 0.42, where pH* is the direct reading from a H_2O-calibrated pH meter.[68] The samples were studied using SANS without any pre-experimental filtration.

SANS measurements were mainly carried out at the D22 beamline of the Institut Laue−Langevin, Grenoble, France, along with supplementary measurements on Larmor and Sans2d at the ISIS Neutron and Muon Source at the Rutherford Appleton Laboratory, Oxford, UK.

At D22, experiments were carried out using a circular neutron beam with a diameter of 13 mm. The wavelength of the neutron beam and the q range investigated were 6 Å ($\Delta\lambda/\lambda$ = 0.1) and 0.002 to 0.641 $Å^{-1}$ respectively. The two different detectors in D22, (i) a fixed front detector and (ii) a rear detector, had sample-to-detector distances of 1.4 and 17.6 m (with a collimation distance of 17.6 m), respectively, enabling access to a wide q range. The neutrons were recorded using ^{3}He multitube detectors made of Reuter−Stokes tubes; the front detector consists of 96 tubes, while the rear one has 128 (tube diameter: 8 mm and a pixel size of 8 mm × 8 mm). Using the GRASP software,[69] the two-dimensional multi-detector data were corrected for direct beam transmission, empty cell scattering, background scattering, and detector efficiencies before being scaled to absolute intensity and azimuthally averaged. Finally, incoherent scattering was subtracted from each averaged dataset obtained.

The measurements performed on the time-of-flight instrument Larmor at the ISIS Neutron and Muon Source used a square beam of 6 × 6 mm with a neutron wavelength range of 0.9−13.5 Å. The sample-to-detector distance of 4.1 m enabled an effective q-range of 0.004−0.680 $Å^{-1}$ (the source-to-detector distance was also set to 4 m). Scattered neutrons were recorded in event mode on a ^{3}He tube array detector (64 × 64 cm^2) with a 4 mm × 8 mm pixel size. The raw data obtained were converted to scattering cross-section data and set onto an absolute scale after being corrected for transmission, empty cell scattering, background scattering, detector efficiencies, and radially averaged using Mantid Workbench software.[70] Further, at Sans2d small-angle neutron diffractometer at ISIS,[71] the beamline operated with a neutron beam diameter of 12 mm, and the wavelength range used was 1.75−16.5 Å. The use of two 1 m^2 detectors at 2.4 and 4 m from the sample provided access to a q-range of 0.004−1 $Å^{-1}$, with a q-resolution varying from ca. 2% at the highest q-values to ca. 19% with decreasing q-values, calculated using the Mildner−Carpenter equation.[72] The same protocol was used to correct the 2D patterns (using transmission, empty cell scattering, background scattering, and detector efficiencies), which were then radially averaged, converted to scattering cross-section data, and absolutely scaled using a standard polymer in the Mantid software.[70] Then, the incoherent scattering was subtracted from all of the corrected scattering curves from ISIS instruments as well.

2.6.6. Light Scattering. Light scattering measurements of the 0.1 wt % aqueous polymer suspensions, gently stirred overnight at the required pH and filtered using 0.45 μm PTFE membrane-based Millipore filters (for the corresponding buffer solutions, 0.22 μm PTFE filters were utilized), were carried out using an ALV CGS3 goniometer with an ALV 5004 correlator (ALV GmbH, Langen, Germany). Multiple tau digital correlators in the equipment allow measurements of static and dynamic light scattering in parallel. The instrument is equipped with a HeNe laser with a wavelength of λ = 632.8 nm and a maximum output power of 23 mW. Samples were measured at 21.5 ± 1.0 °C and at an angular range between 30° and 150°.

Complementary measurements of the effect of salt were carried out on an AMERIGO instrument from Cordouan Technologies, France, using a laser at 638 nm with a laser power of 100% for all samples. Samples (Ami. Pol 5 at pH 5 with [NaCl] ranging from 0 to 1 M) were filtered using 0.8 μm PTFE membrane-based Millipore filters. The data were

https://doi.org/10.1021/acs.macromol.4c02884
Macromolecules 2025, 58, 5110−5134

measured at a scattering angle of 170°. The scattered intensity was averaged over 45 s of measurements.

2.7. Scattering Data Analysis. *2.7.1. Models Used to Fit the SANS Data. 2.7.1.1. Polymer Micelles Model.* The SANS data were fitted using the model of polymer micelles described by Pedersen and Gerstenberg.[73] This model is well-suited to describe micelles made of diblock copolymers, where one block forms the core of the micelle with a radius R and scattering length density (SLD) ρ_{core} and the second block forms a shell with SLD ρ_{shell} made of solvated chains, each with a radius of gyration R_g (see Scheme 2). N_{agg}, the aggregation number, represents the number of copolymers in each micelle, while v_{core} is the volume occupied by one block within the micelle core, and v_{shell} is the volume occupied by one chain in the shell.

Scheme 2. Sketch of a Polymer Micelle of Core Radius R and Shell Block Gyration Radius, R_g

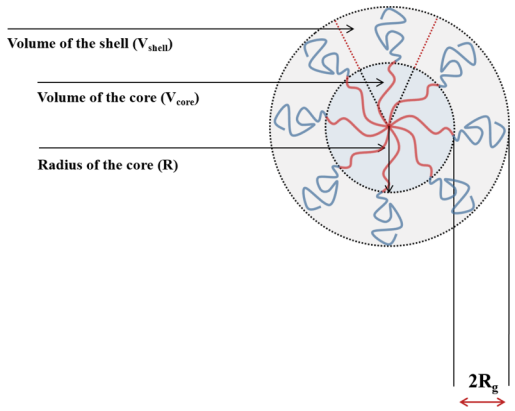

By considering the total volume of the core

$$V_{core} = 4/3\pi R^3 \tag{2}$$

the volume occupied by one block in the core v_{core} can be rewritten as

$$v_{core} = \frac{V_{core}}{N_{agg}} = \frac{^4/_3\pi R^3}{N_{agg}} \tag{3}$$

Moreover, the scattering length densities can be estimated as follows:

$$\rho_{core} = 0.5\rho_{AU} + 0.5\rho_{AA} \tag{4}$$

$$\rho_{shell} = 0.25\rho_{POEGMEA} + 0.75\rho_{D_2O} \tag{5}$$

with ρ_{AU}, ρ_{AA}, $\rho_{POEGMEA}$, and ρ_{D_2O} the SLD of *N*-Acyl urea, acrylic acid, the P(OEGMEA) block, and heavy water, respectively. To simplify the model, we neglected any presence of water within the core, while we estimated the amount of water in the shell to be 75%.[74] We also neglected the possible presence of *N*-Boc-ethylenediamine within the core due to its relatively low amount. Table 4 provides the densities and SLD for each compound and the final SLD estimated for the core and shell.

For noninteracting micelles, the scattered intensity I (cm^{-1}) can be described as follows:

$$I(q) = nP_{mic}(q) \tag{6}$$

with n being the number of objects per unit volume (cm^{-3}) and $P_{mic}(q)$ the form factor of the micelles, with

$$\begin{aligned} P_{mic}(q) &= N_{agg}^2 v_{core}^2 \Delta\rho_{core}^2 P_{sphere}(q, R) \\ &\quad + N_{agg} v_{shell}^2 \Delta\rho_{shell}^2 P_{ch}(q, R_g) \\ &+ N_{agg}(N_{agg} - 1) v_{shell}^2 \Delta\rho_{shell}^2 S_{cc}(q, R, R_g) \\ &+ 2N_{agg}^2 v_{core} \Delta\rho_{core} v_{shell} \Delta\rho_{shell} S_{sc}(q, R, R_g) \end{aligned} \tag{7}$$

where $\Delta\rho_X = \rho_X - \rho_{D_2O}$ is the SLD difference between the object (X = core or shell) and the solvent.

P_{sphere} is the form factor of a simple sphere of radius R that describes the core, with $P_{sphere}(q, R) = F^2_{sphere}(q, R)$, with F_{sphere} is the form factor amplitude:

$$F_{sphere}(q, R) = \frac{3[\sin(qR) - qR\cos(qR)]}{(qR)^3} \tag{8}$$

P_{ch} describes the form factor of 1 polymer chain composing the shell

$$P_{ch}(q, R_g) = P_{ch}(x = (qR_g)^2) = \frac{2[\exp(-x) - 1 + x]}{x^2} \tag{9}$$

while S_{cc} and S_{sc} are cross terms between two different chains and the core and one chain, respectively, arising when passing from the form factor amplitude to the full form factor:

$$S_{cc}(q) = \psi(q, R_g)^2 \left[\frac{\sin(q(R + dR_g))}{q(R + dR_g)}\right]^2 \tag{10}$$

and

$$S_{sc}(q) = F_{sphere}(q, R)\psi(q, R_g)\frac{\sin(q(R + dR_g))}{q(R + dR_g)} \tag{11}$$

with

Table 4. Scattering Length Density of the Components Used in the Copolymer (SLDs of Core and Shell Included)

Component name	Density (g/mL)	SLD (10^{-6}/Å^2)
Oligo(ethylene glycol)methyl ether acrylate (OEGMEA)	1.80	0.719
Acrylic Acid (AA)	1.051	1.45
Acyl urea[a]	1.320	1.19
N-Boc-ethylenediamine	1.012	0.647
$\rho_{core} = 0.5\rho_{AU} + 0.5\rho_{AA}$	---	1.32
$\rho_{shell} = 0.25\rho_{POEGMEA} + 0.75\rho_{D_2O}$	---	4.97

[a]Density of urea used.

https://doi.org/10.1021/acs.macromol.4c02884
Macromolecules 2025, 58, 5110−5134

$$\psi(q, R_g) = \psi(x = (qR_g)^2) = \frac{1 - \exp(-x)}{x} \quad (12)$$

and $0 \leq d \leq 1$, the interpenetration parameter characterizing how much of the outside chain interpenetrates within the core. In our case, we always fixed $d = 1$ (no interpenetration).

The polydispersity in size over the micelle radius R was taken into account using the Schulz–Zimm distribution, i.e.:

$$\langle P(q, R)\rangle_\sigma = \int f_{SZ}\left(r, R, \frac{1}{\sigma^2} - 1\right) P(q, r)dr \quad (13)$$

with

$$f_{SZ}(x, x_0, z) = \frac{x^z}{\Gamma(z+1)}\left(\frac{z+1}{x_0}\right)^{z+1} \exp\left(-(z+1)\frac{x}{x_0}\right) \quad (14)$$

and σ the polydispersity index in %. The Schulz–Zimm distribution was previously used successfully to characterize the polydispersity in size of core–shell micelles.[75]

The model can be adapted to ellipsoidal or even cylindrical polymer micelles.[76]

When studying micelles as a function of concentration, interactions between micelles arise, and the structure factor has to be considered. Due to the complex nature of the model, the intensity cannot be described as the product of the form factor and the structure factor. Instead, the analytical calculation from Pedersen[77] should be used:

$$I = n(P_{mic}(q) + (A_{mic}^{AV}(q))^2[S(q) - 1]) \quad (15)$$

with

$$A_{mic}^{AV}(q) = N_{agg}\left[v_{core}\Delta\rho_{core}F_{sphere}(q, R) + v_{shell}\Delta\rho_{shell}\psi(q, R_g)\frac{\sin(q(R + dR_g))}{q(R + dR_g)}\right] \quad (16)$$

with $A_{mic}^{AV}(q)$ the form factor amplitude of the average radial scattering length density distribution.

The structure factor $S(q)$ was accounted for by a hard-sphere model, using the well-known Percus–Yevick solution.[78] $S(q)$=$S(q, R_{HS}, \varphi_{HS})$ depends on the hard-sphere radius R_{HS} and the volume fraction of interacting micelles φ_{HS}.

Data were fitted using a custom Fortran program.[79]

2.7.1.2. Secondary Models: Guinier Approximation and Polymer Chains with Excluded Volume. In a few cases, shape-independent models were used to characterize the SANS data. The well-known Guinier approximation[80] was used to obtain the radius of gyration R_G of the micelle to compare with SLS data. In the Guinier approximation, the intensity can be written

$$I(q) = A \cdot e^{-q^2R_G^2/3} + B \quad (17)$$

with A as a scaling factor and B as a background term. R_G is not to be confused with the radius of gyration R_g of the P(OEGMEA) chains that compose the shell of the micelles used in the polymer micelles model ($R_G \gg R_g$).

On the other side, when micelles are not formed, the DHBC remains free in suspension. This free polymer was described using the polymer chains with excluded volume model.[81] This model, whose analytical form was given by Hammouda in 1993, depends on the radius of gyration R'_g of the complete polymer chain (i.e., the complete DHBC) in solution and the Porod exponent α that characterizes the signal at high angles ($I \propto q^{-\alpha}$). For a linear polymer in a good solvent, $\alpha \approx 5/3$, but it is higher for comb-like polymers.[22] R'_g is not to be confused with the radius of gyration R_g of the P(OEGMEA) chains that compose the shell of the micelles used in the polymer micelles model ($R'_g \sim R_g$).

Those models are readily available on SasView.

2.7.2. Static Light Scattering. The weight-averaged molecular weight M_w, and radius of gyration of the scattering objects R_G could be obtained from SLS data depicted using Zimm's approximation

$$\frac{Kc}{\Delta R_\theta} = \frac{1}{M_w} + \frac{1}{3M_w}R_G^2q^2 \quad (18)$$

where c and K are the concentration of the scattering objects and the optical constant, respectively, and q is the scattering vector that depends on the scattering angle θ:

$$q = \frac{4\pi n}{\lambda_0}\sin\frac{\theta}{2} \quad (19)$$

The optical constant K can be written as

$$K = \frac{4\pi^2}{\lambda_0^4 N_A}\left(n\frac{dn}{dc}\right)^2 \quad (20)$$

where λ_0, N_A, n, and $\frac{dn}{dc}$ are the laser wavelength in vacuum, Avogadro's number, the refractive index of the solvent, and the refractive index increment of the self-assembled species, respectively. Experimentally, we measured the scattering intensity <I> as a function of the scattering vector, q. The Rayleigh ratio (ΔR_θ) was then obtained using eq 20

$$\Delta R_\theta = \frac{\langle I_{solution}\rangle - \langle I_{solvent}\rangle}{\langle I_{standard}\rangle}\left(\frac{n_{solvent}}{n_{standard}}\right)^2 RR_{standard} \quad (21)$$

with $\langle I_{solution}\rangle$, $\langle I_{solvent}\rangle$, and $\langle I_{standard}\rangle$ representing the scattering intensities of the solution, solvent (i.e., water), and standard (i.e., toluene), respectively. $n_{solvent}$ = 1.33 and $n_{standard}$ = 1.49 are the respective refractive indexes while $RR_{standard}$ = 1.36×10^{-5} cm^{-1} for λ = 632.8 nm at 21.5 ± 1.0 °C is the Rayleigh ratio of the toluene standard.

Plotting $\frac{Kc}{\Delta R_\theta}$ against q^2 shows a linear dependence. The slope ($\frac{R_G^2}{3}$) yields the radius of gyration and the intercept gives the molecular weight ($\frac{1}{M_w}$) of the self-assembled entities. $\frac{dn}{dc}$ value was not determined experimentally. Hence, we extracted only the radius of gyration, R_G. Let us note that the radius of gyration R_G obtained in SLS is different from the radius of gyration of polymer chains in the shell of the micelles R_g from the SANS analysis made using the polymer-micelles model. In SLS, R_G corresponds to the radius of gyration of the scattering objects, which, in most cases, are the micelles. At pH values where micelles are not formed, it would correspond to the radius of gyration of the DHBC soluble in water.

2.7.3. Dynamic Light Scattering. In DLS, we measured the scattered intensity as a function of time at a specific scattering vector, q. From the scattered intensity, the normalized intensity–time correlation function, $g_2(q,\tau)$ is obtained as a function of time shift, τ. Utilizing Siegert's equation, the

https://doi.org/10.1021/acs.macromol.4c02884
Macromolecules 2025, 58, 5110–5134

electric field−time correlation function $g_1(q,\tau)$ could be extracted.

$$g_2(q,\tau) = \frac{\langle I(q,t)I(q,t+\tau)\rangle}{\langle I(q,t)^2\rangle} = 1 + |g_1(q,\tau)|^2 \quad (22)$$

where $I(q,t)$ and $I(q,t+\tau)$ are the scattering intensities at time t and $t+\tau$, respectively. $\langle\ \rangle$ indicates temporal averaging over all the times, t.

The electric field correlation function relates to the particle translational diffusion coefficient, which can be obtained using either the CONTIN method or the cumulant analysis. The latter is well-suited for a quasi-monomodal distribution of population, while the former is better tailored for systems that exhibit several populations.

In CONTIN, developed by Provencher based on the Laplace inverse, the electric field correlation function $g_1(q,\tau)$ is related to the translational diffusion coefficient D_t by

$$g_1(q,\tau) = \int_0^\infty G(D_t)\cdot e^{-D_t\cdot\tau/q^2} dD_t \quad (23)$$

with $G(D_t)$ being the distribution function of D_t.[82]

The cumulant fit describes the logarithm of $g_1(q,\tau)$ at fixed q as a power series in τ,

$$\ln(g_1(q,\tau)) = \Gamma_0 - \Gamma_1\cdot\tau + \frac{\Gamma_2}{2!}\cdot\tau^2 - \frac{\Gamma_3}{3!}\cdot\tau^3 \quad (24)$$

with Γ_0, Γ_1, Γ_2, and Γ_3 as the cumulants. The first cumulant is related to the z-averaged translational diffusion coefficient D through $\Gamma_1 = Dq^2$, while the ratio between the second and the square of the first cumulant unveils the polydispersity index $PDI = \frac{\Gamma_2}{\Gamma_1^2}$.

Here, the translational diffusion coefficient D is obtained at a single scattering vector, q. To extract the translational diffusion coefficient with greater accuracy, it is necessary to study the sample at different scattering vectors and extrapolate the translational diffusion coefficient at zero angle D_0. For dilute solutions, D_0 is calculated using the linear approximation method described below:

$$D = D_0(1 + C\cdot R_g^2\cdot q^2) \quad (25)$$

where C is a dimensionless constant that depends on polydispersity and particle shape. By plotting D as a function of q^2, the intercept allows extracting D_0. If there is no angular dependence, D_0 is obtained by averaging over the angular range.

Once D_0 is obtained, the hydrodynamic radius R_H is calculated via the Stokes−Einstein relationship:

$$R_H = \frac{K_B T}{6\pi\eta}\frac{1}{D_0} \quad (26)$$

with k_B, T, and η denoting the Boltzmann constant, temperature, and solvent viscosity, respectively. Finally, combining static and dynamic light scattering data allows for extracting the shape-reliant ratio $\frac{R_G}{R_H}$.[82−84] Spherical objects usually exhibit a ratio of ca. 0.78.

3. RESULTS AND DISCUSSION

3.1. Parent Block Copolymer, Par. Pol. (P(OEGMEA)-*b*-P(AA)). The parent diblock copolymer, Par. Pol., made of P(OEGMEA)-*b*-P(AA), whose chemical structure is given in Scheme 3, was synthesized by RAFT polymerization following previously established protocols.[55,56] The degree of polymerization of each block was determined using ^{1}H NMR, and the results indicate 24 units of P(OEGMEA) and 53 units of P(AA) (see Table 1), with a monomer conversion rate of ca. 99% for both blocks. This corresponds to a total molecular weight of 15.6 kDa (including the terminal groups) for the DHBC, with contributions of 11.5 kDa and 3.8 kDa from P(OEGMEA) and P(AA), respectively (Figure S1).

Scheme 3. Structure of the Parent Polymer, Par. Pol., P(OEGMEA)$_m$-*b*-P(AA)$_n$

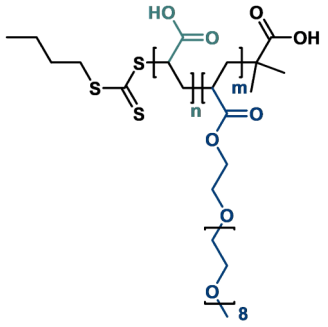

3.2. Modification of the Parent Polymer by Activation and Amidation of the Acrylic Acid Functions. *3.2.1. Activated and Amidated Copolymers, Act. Pol. (P(OEGMEA)-b-P(AA-s-(AA-NHS)-s-(Acyl urea)) and Ami. Pol. (P(OEGMEA)-b-P(AA-s-(Acyl urea)-s-(N-Boc)))*. In order to introduce new functional groups to the ionic block and impart self-micellization capabilities to P(OEGMEA)-*b*-P(AA) copolymers, a specific modification of the P(AA) block was carried out through activation/amidation of the carboxylic acid groups. Since both blocks of the DHBC are based on acrylate monomers, mild reaction conditions were necessary to achieve specific reactions on the polyacid block P(AA) while leaving the comb polyester block P(OEGMEA) untouched. Additionally, since the copolymer synthesis was achieved in water, an aqueous functionalization route was favored to reduce the environmental impact of the synthesis. Activation of carboxylic acid groups was achieved through successive reactions with 1-ethyl-3-(3-(dimethylamino)propyl) carbodiimide (EDC) and *N*-hydroxysuccinimide (NHS) in order to achieve two aims: (i) forming reactive esters P(OEGMEA)-*b*-(PAA-NHS) for subsequent amidation and (ii) forming stable N-Acyl urea pendant functions P(OEGMEA)-*b*-(PAA-Acyl urea), which contain a tertiary amine (pK_{aH} = 9.76). The presence of amine functions, together with acrylate functions, may induce intramolecular complexation-driven self-micellization of the newly formed DHBC.

Indeed, while the reaction of EDC on carboxylic acid forms *O*-Acyl urea esters, these moieties can undergo hydrolysis or, more importantly, rearrangement (N → O displacement) before reacting with NHS. As a result, AA and *N*-Acyl urea-grafted AA are obtained, respectively. These side reactions are typically controlled by NHS addition, as it reacts with *O*-Acyl urea esters to give an activated ester that can conveniently react with primary amines.[59] In contrast, the *N*-Acyl urea and carboxylic acid side products do not react with primary amines under mild conditions. Here, in our amidation protocol, after EDC was added, there was a subsequent delay before NHS

https://doi.org/10.1021/acs.macromol.4c02884
Macromolecules 2025, 58, 5110−5134

Scheme 4. 4a (a) Step 1: Activation of Par. Pol. ($P(OEGMEA)_m$-*b*-$P(AA)_n$) into Act. Pol. (P(OEGMEA)-*b*-P(AA-*s*-(AA-NHS)-*s*-(Acyl urea))); (b) Step 2: Amidation of Act. Pol. (P(OEGMEA)-*b*-P(AA-s-(AA-NHS)-*s*-(Acyl urea))) into Ami. Pol. (P(OEGMEA)-*b*-P(AA-*s*-(Acyl urea)-*s*-(*N*-Boc)))

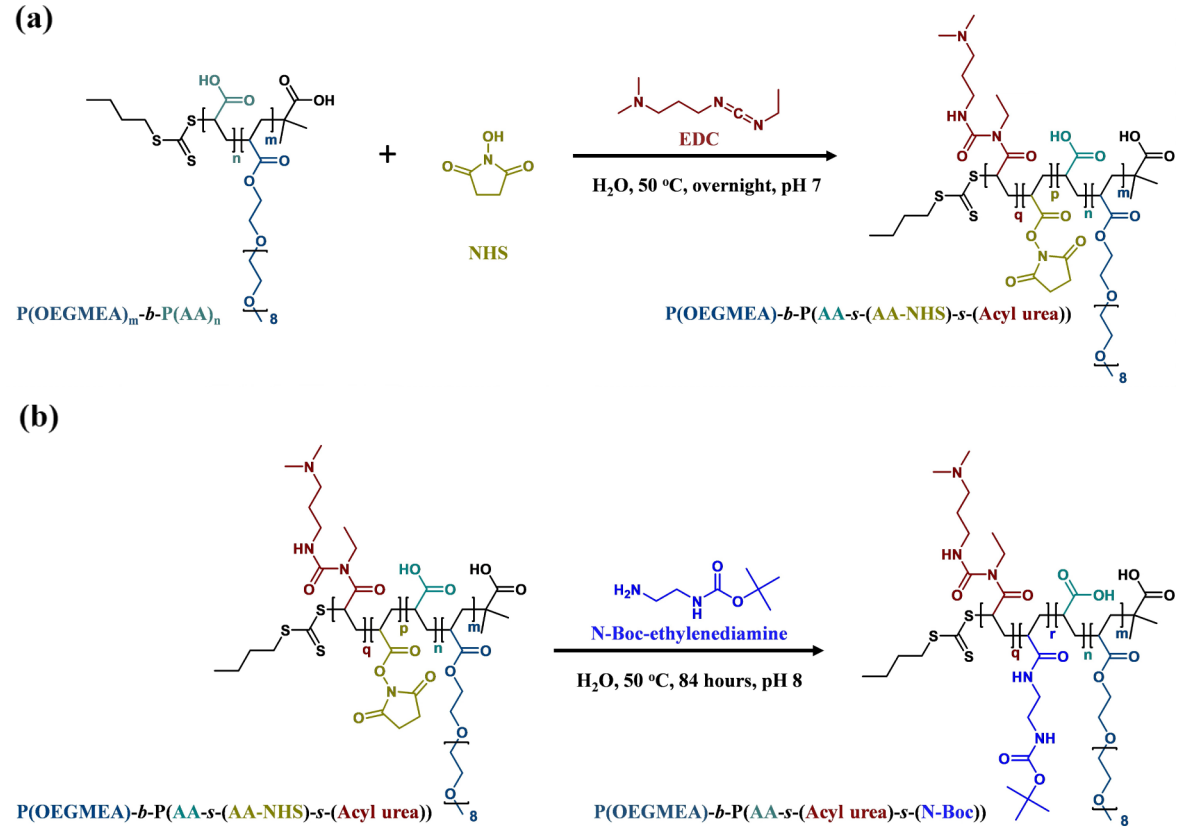

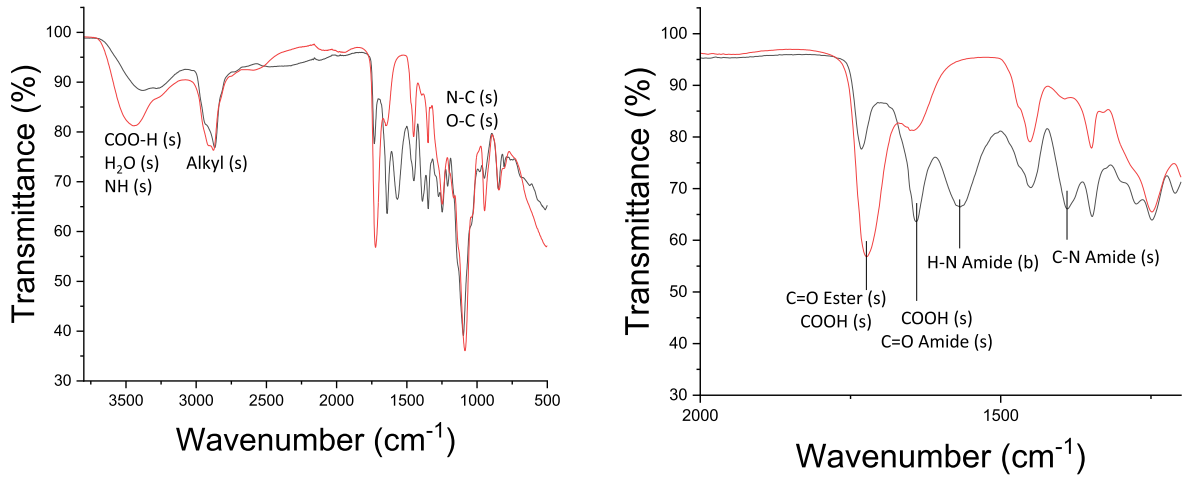

Figure 1. ATR-FTIR spectra of Par. Pol. (red line) and Ami. Pol. 1 (black line) (a) over the entire wavenumber range and (b) over 2000−900 cm^{-1}. The main band contributions have been highlighted, with each time the type of vibration ((s) for stretching, (b) for bending).

addition to the reaction medium in order to ensure the formation of both stable *N*-Acyl urea and activated ester. Sam et al. in their study of the EDC/NHS activation of acid end groups (at 15 °C for 1.50 h in water), reported that the excess of added EDC and NHS favors rearrangement and formation of *N*-Acyl urea rather than the activated ester.[43] Hence, in this study, an excess of EDC and NHS (excess ratio of ca. 1.70 for both) was used for the activation of the parent copolymer. Therefore, the typical activated copolymer, Act. Pol., obtained has a fraction of the three possible products, giving P(OEGMEA)-*b*-P(AA-*s*-(AA-NHS)-*s*-(Acyl urea)), see Scheme 4a. To graft primary amines on the DHBC, the activated copolymer was subsequently reacted with *N*-Boc-ethylenediamine, forming the amidated copolymer or Ami. Pol. exhibiting both N-Boc-protected amine and *N*-Acyl urea pendant groups, with the following chemical formula, P(OEGMEA)-*b*-P(AA-*s*-(Acyl urea)-*s*-(*N*-Boc)), see Scheme 4b.

Although amidation of carboxylic acids can be achieved by direct reaction with primary amines, it is virtually impossible to

https://doi.org/10.1021/acs.macromol.4c02884
Macromolecules 2025, 58, 5110−5134

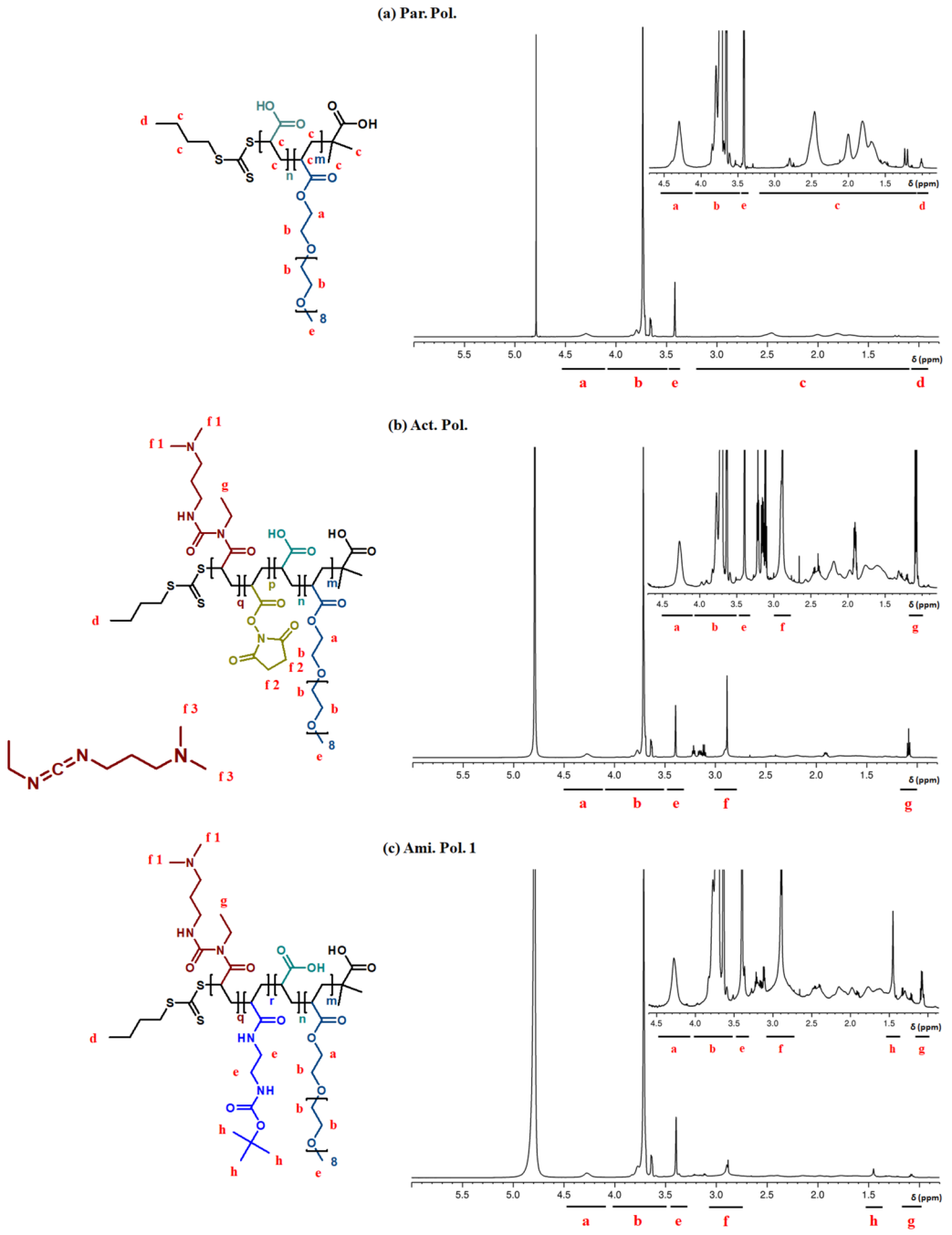

Figure 2. NMR spectra of (a) the parent copolymer P(OEGMEA)$_{24}$-*b*-P(AA)$_{53}$ (Par. Pol.) and b) the activated polymer, P(OEGMEA)$_{24}$-*b*-P((AA)$_{25}$-*s*-(AA-NHS)$_{17}$-*s*-(Acyl urea)$_{11}$) (Act. Pol.) and (c) amidated polymer, P(OEGMEA)$_{24}$-*b*-P((AA)$_{28}$-*s*-(Acyl urea)$_{17}$-*s*-(*N*-Boc)$_8$) (Ami. Pol. 1). The number of units for each groups were calculated using the peaks highlighted using alphabetical characters. The insets, showing the chemical formula of each copolymer, indicate the protons attribution to each peak. The peak at 4.30 ppm is used for calibration.

accomplish in water because the chemical equilibrium strongly favors the hydrolysis of the acid groups. To overcome this problem, direct amidation in the absence of EDC/NHS activation requires high temperatures (160 °C−180 °C), which would lead to the alteration of both blocks in the case of a P(OEGMEA)-*b*-P(AA) copolymer.[59] Therefore, activation of the copolymer using the above protocol is essential for achieving both amidation and grafting of *N*-Acyl urea groups onto DHBC under mild and aqueous conditions.

3.2.2. ATR-FTIR Analysis. The polymers before (Par. Pol.) and after amidation (Ami. Pol. 1) were studied by ATR-FTIR (Figure 1). After amidation, new bands can be observed between ca. 1500 and 2000 cm^{-1} characteristics of H−N and C═O bonds in amides, proving successful amidation of the P(AA) block. Furthermore, the signal at ca. 1700 cm^{-1}, associated notably with the carbonyl stretching in the esters of the P(OEGMEA) block, is still present after amidation, suggesting the first block was not damaged by the procedure. On top of those bands, the rest of the pattern is similar before and after amidation (notably the presence of alkyls groups between 2800−3000 cm^{-1} and O−C stretching from ethylene glycol units at around 1050 cm^{-1}), again hinting at the absence of damage to the copolymer. A quantification of the modification of DHBC was made using ^{1}H NMR.

https://doi.org/10.1021/acs.macromol.4c02884
Macromolecules 2025, 58, 5110−5134

3.2.3. NMR Analysis. Figure 2 shows the ^{1}H NMR spectra of (a) the parent copolymer P(OEGMEA)-*b*-P(AA) (b) the activated copolymer P(OEGMEA)-*b*-P(AA-*s*-(AA-NHS)-*s*-(Acyl urea)), and (c) the amidated copolymer P-(OEGMEA)-*b*-P(AA-*s*-(Acyl urea)-*s*-(*N*-Boc)) labeled Par. Pol., Act. Pol., and Ami. Pol. 1, respectively (see Tables 1 and 2). In Figure 2, the insets highlight, for each copolymer, the relevant protons corresponding to the peaks used to characterize the copolymer (labeled (a) to (h)).

In all three NMR spectra, the peaks between 0.2−3.2 ppm are predominantly contributions from the acrylate backbone of the copolymer (protons identified as (c)), while the peaks in the range 3.2−4.4 ppm are ascribed to the protons from the oligo(ethylene oxide) methyl ether comb in the P(OEGMEA) block (a, b,e). In particular, the distinct peak at 4.30 ppm is attributed to the two α-hydrogen atoms adjacent to the ester bond in P(OEGMEA) (a).

In Figure 2b, a triplet at ca. 1.2 ppm, from the protons of the methyl end group of *N*-Acyl urea and labeled as (g) allows for the extraction of the number of units of *N*-Acyl urea in the activated copolymer (which gives a conversion rate of ca. 20% for Act. Pol.). Furthermore, the prominent peak at 2.90 ppm could be a collective contribution from three different types of protons: the protons in the tertiary amine group of the N-Acyl urea (f1), the same protons from the tertiary amine of EDC present in excess and not removed by dialysis, and the equivalent protons in the NHS ring (f2), making it impossible to discriminate the signal from both NHS and free EDC at this stage.

In Figure 2c associated with the spectrum of Ami. Pol. 1, four series of peaks can be noted: first, the same triplet at 1.2 ppm related to the methyl group of *N*-Acyl urea (*g*) allows the number of *N*-Acyl urea groups to be extracted in the copolymer. Second, the peak at 2.90 ppm is associated with the protons in the tertiary amine group of *N*-Acyl urea and the same protons on EDC in excess (f). Indeed, we assume all the NHS-activated sites to have been either hydrolyzed or amidated. A zoom on the peak at 2.90 ppm reveals that it is composed of a broad peak (probably from protons of the immobilized *N*-Acyl urea groups) and a sharp peak (from the same protons but on the remaining EDC), proving that EDC in excess is not fully removed after dialysis but is not covalently attached to the DHBC. Once the contribution from *N*-Acyl urea is known, this peak can hence be used to extract the amount of EDC still present. Third, another peak at 1.47 ppm corresponds to the *tert*-butyl group in the *N*-Boc-ethylenediamine group (h). Finally, the peak at ca. 3.4 ppm is this time not only due to the 3 protons of the methyl terminal group of the P(OEGMEA), but also from the 4 protons before the amine function in the Boc pending group (e). These last two peaks (h and e) provide two methods to extract the number of *N*-Boc pending groups, and we took the average.

Using the peak at 4.30 ppm in the spectrum of Ami. Pol. 1, P(OEGMEA)-*b*-P(AA-*s*-(Acyl urea)-*s*-(*N*-Boc)), for calibration, the conversion rates of acrylic acid to *N*-Acyl urea and amide groups were found to be ca. 32% and ca. 15%, respectively. Hence, Ami. Pol. 1 may be described as $P(OEGMEA)_{24}$-*b*-$P((AA)_{28}$-*s*-$(Acyl\ urea)_{17}$-*s*-$(N\text{-}Boc)_8)$. It is worth noting that a strong contribution from non-covalently bound EDC can still be observed, as for one DHBC, 11 EDC molecules contribute to the NMR pattern. The relative abundances of the three possible units obtained after the transformation of AA groups, statistically arranged in the ionic block of the copolymers, have been quantified for all samples (see Table 2). In order to confirm the percentage values of activation and amidation, it is essential to verify that the P(OEGMEA) block is not damaged during the amidation step. Therefore, the peak at 4.30 ppm was again used as the reference (corresponding to the two α-hydrogens adjacent to the ester bond in P(OEGMEA), labeled a) to determine the area of the peak between 3.6−4.0 ppm before and after amidation. Similar values were obtained, confirming the absence of damage (Figure S2), in agreement with ATR-FTIR results.

After amidation, the copolymers contain an unmodified P(OEGMEA) polyester block and a transformed P(AA) block containing randomly distributed protected amine species, tertiary amine species, and acrylic acid units. For moderate pH values, the resulting P(OEGMEA)-*b*-P(AA-*s*-(Acyl urea)-*s*-(N-Boc)) copolymer thus simultaneously presents positive and negative charges.

3.2.4. Elemental Analysis. The activated and amidated copolymers were characterized using elemental analysis (EA) to determine their CHNS composition. The primary purpose of these results (presented in Tables 2 and S1) was to complement the NMR analysis in accurately determining the relative abundance of each possible product unit within the P(AA) block after activation with EDC/NHS (Act. Pol.) and subsequent amidation with *N*-Boc-ethylenediamine (Ami. Pol. 1−4), which introduced protected amine species into the poly(acrylic acid) block. In the case of Act. Pol., which corresponds to P(OEGMEA)-*b*-P(AA-*s*-(AA-NHS)-*s*-(Acyl urea)), the measured weight percentages were 46.95% carbon, 8.79% hydrogen, and 6.08% nitrogen, yielding atomic ratios of N/C = 0.111 and H/C = 2.25. As the amount of *N*-Acyl urea pendant groups is known from NMR, these elemental ratios within the copolymer were used to estimate the amount of activated ester groups. Act. Pol. was thus characterized as $P(OEGMEA)_{24}$-*b*-$P((AA)_{25}$-*s*-$(AA\text{-}NHS)_{17}$-*s*-$(Acyl\ urea)_{11})$, complementing the NMR measurements. In the amidated copolymers P(OEGMEA)-*b*-P(AA-*s*-(Acyl urea)-*s*-(*N*-Boc)) (Ami. Pol. 1−4), the obtained atomic ratios typically indicated equal or higher nitrogen content compared to the activated copolymer. For example, in Ami. Pol. 1, atomic ratios determined by elemental analysis were found to be N/C = 0.132 and H/C = 2.28 (from 48.84% carbon, 9.28% hydrogen, and 7.52% nitrogen weight ratios). These values are in relatively good agreement with the calculated atomic ratios based on the number of units deduced from NMR data, while accounting for the contribution from EDC not removed by dialysis (N/C_{NMR} = 0.102 and N/C_{EA} = 0.132). This approach of cross referencing data between NMR and EA analysis was applied to Ami. Pol. 1−4 (see Table 2). It is worth noting that ratios from EA are consistently found to be slightly higher than the calculations made from the number of units obtained by NMR pattern analysis, likely due to an underestimation of the amount of EDC impurities in the sample.

Elemental analysis, along with NMR, fully confirms the incorporation of amine entities in the activated and amidated copolymers. The highest *N*-Acyl urea content is recorded in Ami. Pol. 2 (32%) and the lowest in Ami. Pol. 4 (13%). For Act. Pol., Ami. Pol. 1 and Ami. Pol. 3, the conversion rates to *N*-Acyl urea are found to be 21%, 32%, and 23%, respectively (see Table 2). These results may be related to the pH of the suspension during the addition of EDC and NHS (pH_{act}), as the activation step for Ami. Pol. 2 was carried out at pH_{act} = 7,

https://doi.org/10.1021/acs.macromol.4c02884
Macromolecules 2025, 58, 5110−5134

Scheme 5. Deprotection of Ami. Pol. (P(OEGMEA)-*b*-P(AA-s-(Acyl urea)-*s*-(N-Boc))), to Obtain the Targeted Deprotected Polymer, De. Pol., (P(OEGMEA)-*b*-P(AA-*s*-(Acyl urea)-s-(AA/NH_2)))

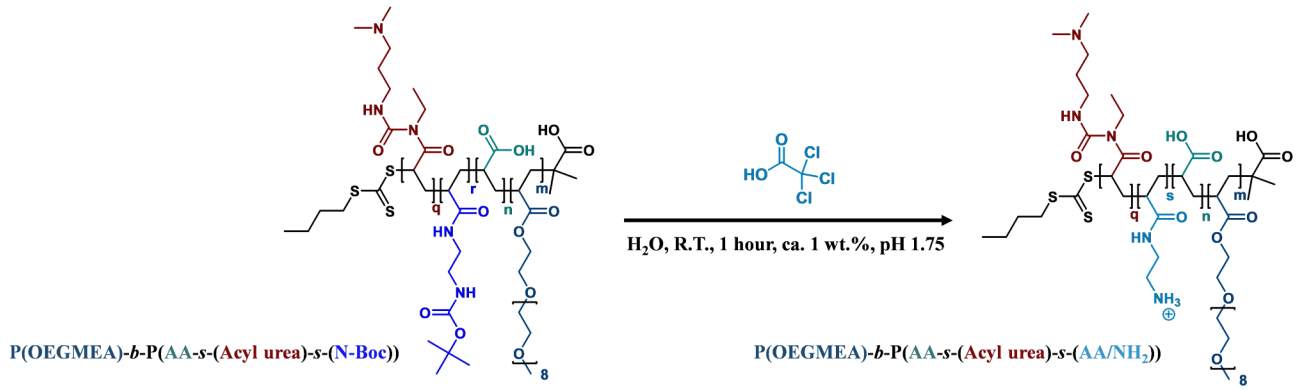

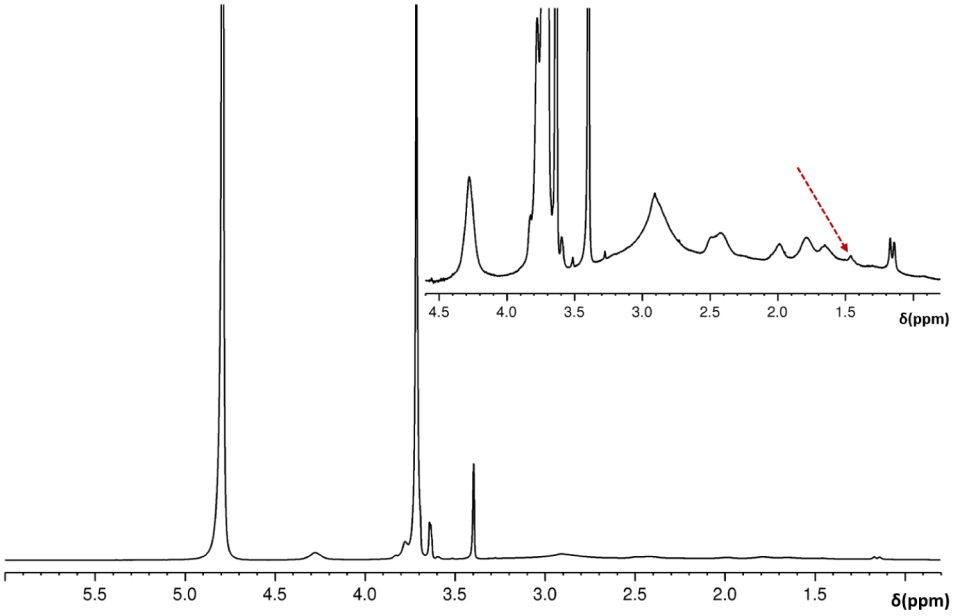

Figure 3. 1H NMR spectra of De. Pol. 1 from the deprotection of Ami. Pol. 1. The graduation in red (1.47 ppm) is the position where a peak associated with the 9 protons of the *tert*-butyl group would be seen, highlighting its absence.

while Ami. Pol. 4 and Ami. Pol. 3 were done at pH_{act} = 8 and 9, respectively. The activation pH chosen could influence the balance between NHS and *N*-Acyl urea grafting and, hence, the final ratio of *N*-Acyl urea. It is noteworthy that Ami. Pol. 1, 2, and 5, all activated at pH = 7, show the same conversion rate to *N*-Acyl urea, proving the consistency of the method. Additionally, having a longer activation step (t_{act}) does not improve the final *N*-Acyl urea content, as Ami. Pol. 2 was activated for 15 min before *N*-Boc-ethylenediamine addition, while Ami. Pol. 1 was activated overnight, without a significant alteration in the amount of *N*-Acyl urea content in the amidated polymer. Finally, the activated copolymer shows a lower conversion rate, probably because some *o*-Acyl urea groups are removed during dialysis prior to their modification into *N*-Acyl urea. Furthermore, Ami. Pol. 1, 2, 3, 4, and 5 also reported 15%, 15%, 34%, 26%, and 8% *N*-Boc conversions rates, respectively (see Table 2). Ami. Pol. 1 and 2 exhibit the same amidation rate, showing that a longer activation time t_{act} has little influence on this. However, the higher amidation rates for Ami. Pol. 3 and 4 compared to Ami. Pol. 1, 2, and 5 hint again at the role of pH both during the activation (pH_{act}) and, most importantly, the amidation step (pH_{amid}), with basic pH (9 and especially 8) favoring higher conversion rates. This trend may be rationalized by the better nucleophilic character of *N*-Boc-ethylenediamine under pH conditions that are more favorable for the existence of unprotonated amines. Controlling the activation and amidation steps will be crucial to tailoring the number of *N*-Acyl urea and primary amines available in the final copolymer.

3.3. Deprotection of P(OEGMEA)-*b*-P(AA-*s*-(Acyl urea)-*s*-(*N*-Boc)). *3.3.1. Deprotected Copolymer, De. Pol. (P(OEGMEA)-b-P(AA-s-(Acyl urea)-s-(AA/NH_2)).* In order to free the primary amine groups grafted with *N*-Boc-ethylenediamine, deprotection of the copolymer was carried out by selective acidic hydrolysis of the *N*-Boc protective group. This was achieved by adding trichloroacetic acid (TCA) to a suspension of the amidated copolymer at ca. 1 wt % until a pH of 1.75 was reached. These acidic conditions were maintained for one hour at room temperature. The success of the deprotection was assessed by verifying the removal of *tert*-butyl from the Boc group using NMR spectroscopy. The deprotected copolymer thus presents both primary and tertiary

https://doi.org/10.1021/acs.macromol.4c02884
Macromolecules 2025, 58, 5110−5134

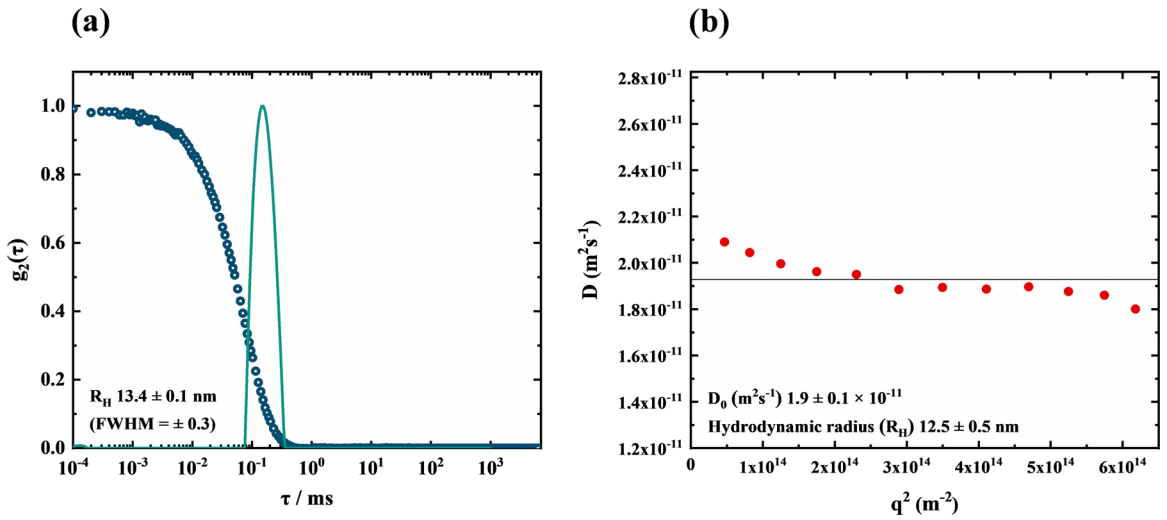

Figure 4. SLS/DLS data of Act. Pol. at 0.1 wt % and pH 5 in H_2O: (a) Intensity−time autocorrelation function $g_2(\tau)$ measured at a scattering angle $\theta = 90°$ and its distribution of relaxation times from the CONTIN analysis (in inset, the associated hydrodynamic radius R_H and full width at half maximum (FWHM) are given). (b) Diffusion coefficient D as a function of the scattering angle from the second order Cumulant analysis. The black line is associated to the average value D_0 given in inset, with the corresponding hydrodynamic radius R_H.

amines as pendant groups in its P(AA) block, yielding P(OEGMEA)-*b*-P(AA-*s*-(Acyl urea)-*s*-(AA/NH_2)), see Scheme 5.

3.3.2. Characterization Using NMR and Elemental Analysis. The deprotection of Ami. Pol. 1 using TCA for 1 h (see Table 3), yielding the copolymer labeled De. Pol. 1, was confirmed initially using ^{1}H NMR, with the disappearance of the peak at 1.47 ppm associated with the 9 protons from the *tert*-butyl group of Boc, see Figure 3. A complete disappearance of this peak contribution was found, suggesting total deprotection. In addition, NMR analysis showed that the contribution from protons of the P(OEGMEA) block was unchanged, indicating that the deprotection conditions did not lead to hydrolysis of the polyester comb. Finally, the contribution from EDC impurities, although still present, was found to be much lower than before deprotection (11 EDC for 1 DHBC before deprotection, whereas only 2 are measured after), proving that the acidic treatment followed by further dialysis helps remove these impurities. The abundance of nitrogen in the copolymer composition was checked using elemental analysis, where 50.77% carbon, 8.95% hydrogen, and 6.79% nitrogen weight fractions were found (De. Pol. 1, Table S2). The high nitrogen content even after deprotection confirms that the amide links on the P(AA) block remain intact even at the low pH of 1.75 used for the deprotection. The atomic N/C ratio obtained from elemental analysis decreased after deprotection: it changed from N/C = 0.132 before deprotection (Ami. Pol. 1) to 0.114 (De. Pol. 1), again hinting at the removal of extra impurities such as EDC. Assuming all the Boc groups are removed, we can use the number of units obtained before deprotection (from Ami. Pol. 1) and the number of units of EDC still present in the sample to calculate an atomic ratio N/C = 0.0844, which is again lower than the actual ratio found in elemental analysis. To further explore the deprotection step, we compared, using Ami. Pol. 2 as polymer, 3 deprotection procedures: TCA for 1 h, TCA for 1 day, or HCl for 1 day. In all cases, the Boc groups were successfully removed as seen by NMR (see Figure S3), and the elemental analysis showed an atomic N/C ratio lower after deprotection (see Table 3).

We previously evidenced the presence of some EDC impurities in the activated and amidated DHBC. Note that due to the electrostatic nature of the interactions between acrylate species and these impurities, a full removal of those impurities by dialysis would require a pH of at least 2 to avoid the formation of micelles that could entrap these impurities in the core (see Section 3.4). However, the different deprotection tests indicate that it is not possible to reach such pH levels without also removing the Boc groups, which is why dialysis at a pH not lower than 3 was carried out with the amidated copolymers.

3.4. Self-Assembly Properties of the Different Polymers Studied via Static and Dynamic Light Scattering and Small-Angle Neutron Scattering. The addition of *N*-Acyl urea and *N*-Boc-ethylenediamine groups to the DHBC may both drastically influence its behavior in solution, notably by imparting self-assembling properties to the activated or amidated copolymers. Specifically, *N*-Acyl urea bears positive charges at pH < pK_{aH} of the tertiary amine,[60,85] while the *tert*-butyl group of *N*-Boc-ethylenediamine is recognized for its hydrophobicity.[53] Both phenomena could, therefore, induce self-assembling properties in the copolymer in aqueous solution, which were investigated using light and small-angle neutron scattering.

3.4.1. Characterization of Par. Pol. and Act. Pol.: Emergence of Self-Assembling Mechanisms After Polymer Modification. The parent copolymer, Par. Pol. (P(OEGMEA)-*b*-P(AA)), is double-hydrophilic and lacks the ability to self-assemble (as confirmed by dynamic light scattering, Figure S5); it requires an external additive, such as a polyion of opposite charge, to induce a coassembly process and form polyion complex micelles.

However, modification of the macromolecule by activation with EDC/NHS gives a copolymer that can self-assemble naturally. As a first step, Act. Pol. was studied to determine the influence of *N*-Acyl urea tertiary amine groups in the P(AA) block on the self-assembled micellar structures. The autocorrelation function $g_2(\tau)$ of intensity vs time and the corresponding relaxation time distributions were measured using DLS at pH 5 and a scattering angle of 90°. Results are

https://doi.org/10.1021/acs.macromol.4c02884
Macromolecules 2025, 58, 5110−5134

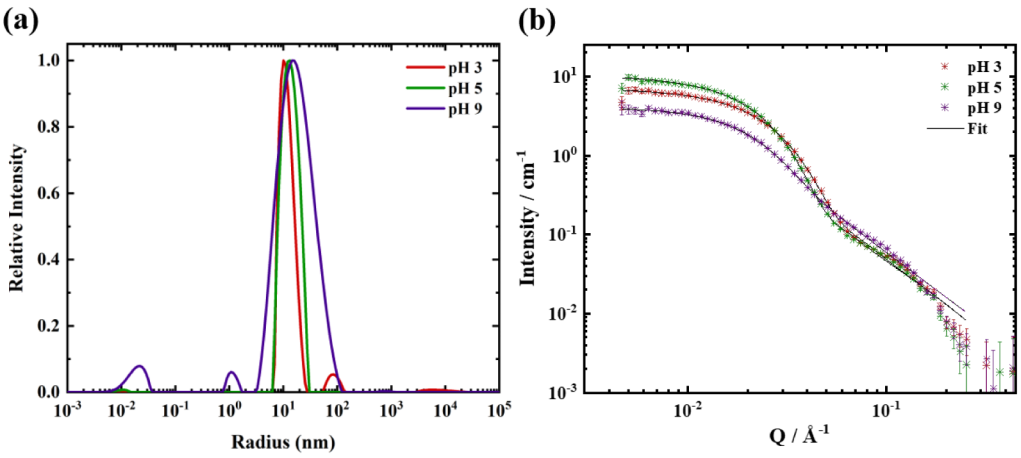

Figure 5. (a) Distribution of sizes of Act. Pol. micelles (0.1 wt %) obtained from the CONTIN analysis of intensity-time autocorrelation functions $g_2(\tau)$ studied at a scattering angle of $\theta = 90°$ and at 3 different pHs in H_2O (associated correlograms are provided in Figure S8) and (b) SANS data of Act. Pol. suspensions (1 wt %) at the same pHs in D_2O. In (b), the fit using the polymer micelle model is shown as black lines.

Table 5. Parameters Obtained from the SANS Data Fitting Using the Model of Polymer Micelles for Suspensions at 1 wt % and Various pHs of 3 Different Polymers: Act. Pol., Ami. Pol. 1, and De. Pol. 1[a,b]

							Structural factor	
Sample name	pH	Scale	Radius, R, nm	Radius of gyration, R_g, nm	Volume of shell, v_{shell}, nm^3	Polydispersity, σ, %	Volume fraction, %	Hard sphere radius, nm
$P(OEGMEA)_{24}$-*b*-$P((AA)_{25}$-*s*-(Acyl urea)$_{11})$	3	0.40×10^{-7} (0.06×10^{-7})	4.3 (0.2)	1.6 (0.2)	0.12×10^{-3} (0.02×10^{-3})	37 (1)	---	-----
	5	0.48×10^{-7} (0.03×10^{-7})	5.2 (0.3)	1.8 (0.2)	0.14×10^{-3} (0.02×10^{-3})	36 (1)	---	----
	9	0.82×10^{-7} (0.88×10^{-7})	4.4 (1.3)	0.6 (0.1)	0.64×10^{-3} (0.48×10^{-2})	74 (30)	----	-----
$P(OEGMEA)_{24}$-*b*-$P((AA)_{28}$-*s*-(Acyl urea)$_{17}$-*s*-(*N*-Boc)$_8)$ (Ami. Pol. 1)	3	0.65×10^{-8} (0.83×10^{-8})	3.5 (0.1)	2.1 (0.1)	0.75×10^{-3} (0.85×10^{-3})	55 (3)	----	----
	4	0.29×10^{-6} (0.06×10^{-6})	3.3 (0.2)	3.6 (0.1)	0.26×10^{-3} (0.01×10^{-2})	28 (5)	----	----
	5	0.14×10^{-6} (0.01×10^{-6})	6.3 (0.1)	3.2 (0.1)	0.72×10^{-2} (0.02×10^{-2})	13 (2)	----	-----
	6	0.15×10^{-6} (0.01×10^{-6})	6.5 (0.1)	2.5 (0.1)	0.84×10^{-2} (0.02×10^{-2})	36 (2)	----	-----
	7	0.16×10^{-6} (0.01×10^{-6})	5.7 (0.1)	3.9 (0.1)	0.86×10^{-2} (0.01×10^{-2})	16 (2)	6 (1)	19.4 (0.2)
	8	0.20×10^{-6} (0.01×10^{-6})	4.7 (0.1)	4.2 (0.1)	0.70×10^{-2} (0.01×10^{-2})	22 (4)	5 (1)	18.1 (0.3)
	9	0.26×10^{-6} (0.03×10^{-6})	3.8 (0.4)	4.5 (0.1)	0.52×10^{-2} (0.03×10^{-3})	32 (11)	5 (1)	17.8 (0.5)
$P(OEGMEA)_{24}$-*b*-$P((AA)_{28}$-*s*-(Acyl urea)$_{17}$-*s*-$(AA/NH_2)_8)$ (De. Pol. 1)	3	0.39×10^{-7} (0.01×10^{-7})	4.0 (0.2)	1.5 (0.2)	0.12×10^{-3} (0.02×10^{-3})	40 (1)	----	----
	4	0.19×10^{-6} (0.01×10^{-6})	5.3 (0.1)	3.5 (0.1)	0.62×10^{-2} (0.01×10^{-2})	17 (1)	5 (1)	15.0 (0.2)
	9	0.49×10^{-7} (0.07×10^{-7})	5.3 (0.3)	1.4 (0.3)	0.13×10^{-3} (0.01×10^{-3})	37 (1)	----	---

[a]Table S4 compares the micelle dimensions probed by DLS and SANS. [b]For each parameter, the standard error is provided between parentheses.

depicted in Figure 4a. The CONTIN fit shows a single peak corresponding to a stable and well-defined population of colloids with a hydrodynamic radius of $R_H = 13.4 \pm 0.3$ nm at pH 5. The data were analyzed at different scattering angles (Figure 4b) to extract more precisely the translational diffusion coefficient of the particles. D_0 was obtained via averaging over the angular range (see Materials and Methods). This gave D_0 ($m^2 \cdot s^{-1}$) = $(1.9 \pm 0.1) \times 10^{-11}$ $m^2 \cdot s^{-1}$ and hence the hydrodynamic radius was found at $R_H = 12.5 \pm 0.5$ nm. The sample was also studied by SLS, and fitting of the Zimm plot was attempted to extract the radius of gyration of the scattering particles R_G (Figure S6). Nevertheless, the SLS data show that R_G is very small ($\ll \lambda/20$); the scattering intensity was found to be independent of the scattering vector, which prevents extracting an accurate value. To calculate R_G/R_H and get some indication of the topology of the species, we hence have to rely on small-angle neutron scattering. The SANS data for the same sample, Act. Pol., measured at 1 wt % in D_2O were therefore fitted first using the Guinier model to extract the radius of gyration of particles R_G (Figure S7). At pH 5, R_G was found to be 7.8 ± 0.1 nm, acquired in the very low q region ($0.004 < q < 0.016$ Å^{-1}) of the scattering curve. This gives a ratio $R_G/R_H = 0.62 \pm 0.03$, which corresponds to spherical species with a nonhomogeneous distribution, as usually seen for micelles.

https://doi.org/10.1021/acs.macromol.4c02884
Macromolecules 2025, 58, 5110−5134

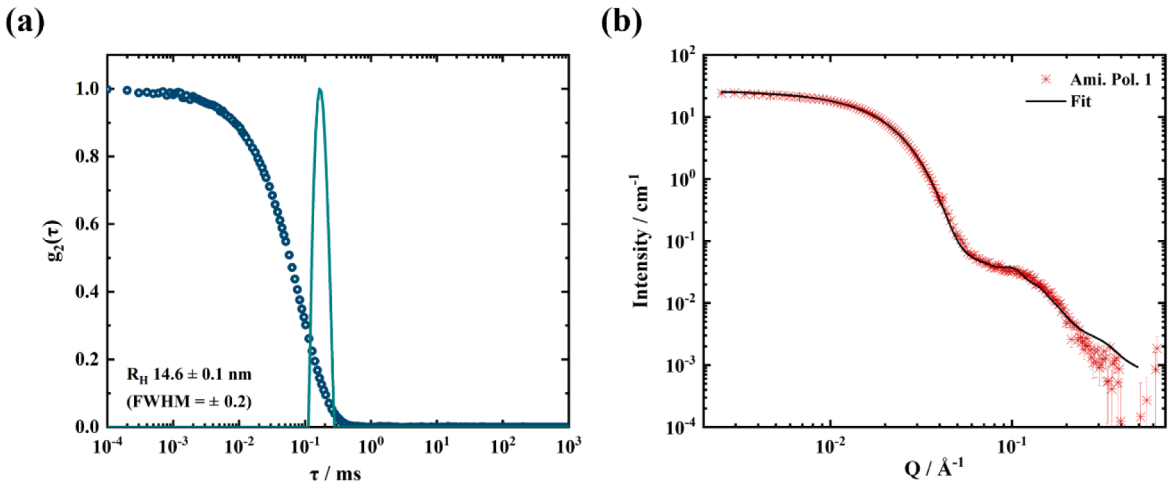

Figure 6. (a) Intensity−time autocorrelation function $g_2(\tau)$ of Ami. Pol. 1 at 0.1 wt % and pH 5 in H_2O, measured at a scattering angle θ = 90 ° and its distribution in relaxation time from the CONTIN analysis (in inset, the associated hydrodynamic radius R_H and full width at half-maximum (FWHM) are given). (b) SANS pattern of Ami. Pol. 1 at 1 wt %, pH 5 in D_2O. In black, the fit made using the polymer micelle model.

The values of R_G, R_H, and the R_G/R_H ratio all suggest that micelles have spontaneously formed from the self-assembly of Act. Pol. alone at pH 5.

Considering that Act. Pol., P(OEGMEA)-*b*-P(AA-*s*-(AA-NHS)-*s*-(Acyl urea)), contains both weak acid (pK_a (AA monomer) = 4.30) and basic (Acyl urea pK_{aH} = 9.76) sites, the effect of pH on the stability, shape, and size of the micellar species was studied using DLS at 90° under three different pH conditions: pH = 3 (acidic conditions), pH = 5, and pH = 9 (alkaline conditions). This pH window prevented any hydrolysis of the copolymer during the experiment. The data obtained were fitted using CONTIN analysis to determine the particle size distributions (Figure 5a). The emergence of a second small population at pH = 3 (R_H = 84.3 ± 0.2 nm) and the significant increase in polydispersity at pH = 9 both indicate a pH-sensitive character of the micellization, which we attribute to electrostatic interactions between the tertiary amine and the carboxylate groups of the diblock.

Small-angle neutron scattering (SANS) experiments were performed on Act. Pol. at the same pH values to further confirm the results obtained from light scattering (Figure 5b). For all pH levels, the signal in the low q region (0.005 < q < 0.040 Å^{-1}) is characteristic of quasi-spherical objects, with a plateau at the smallest angles and an decrease at ca. 0.010−0.020 Å^{-1}. Using the Guinier approximation, we find radii of gyration of micelles (R_G) of 7.1 ± 0.1, 7.8 ± 0.1, and 8.1 ± 0.2 nm at pH = 3, 5, and 9, respectively. Furthermore, the very low q region (0.004 < q < 0.010 Å^{-1}) displays a clear plateau and the absence of an upturn, confirming no aggregation in all three solutions. At higher values of q (0.120 < q < 0.430 Å^{-1}), the data show a power-law dependence $I \sim q^{-\alpha}$ with an exponent α of ca. 2.77, 3.23, and 3.45 at pH = 3, 5, and 9, respectively. This slope could be related to the contribution from polymer chains in the shell of the micelles. Indeed, in the case of comb-like chains such as P(OEGMEA) forming the micelle shell, the slope is higher than in the case of linear polymers in a good solvent, where it is typically α = 5/3.[86] For that reason, the data were fitted using the model for the polymer micelle described in the Materials and Methods section. This model is well-suited for micelles made of block copolymers, notably to accurately describe the shell of micelles (Scheme 2).

Compared to the optimum pH of 5, the scattering intensity shows a noticeable decrease in the low to medium q region (0.010 < q < 0.050 Å^{-1}) for pH = 3 and pH = 9, with an even more pronounced decrease for the latter. This phenomenon could be due to fewer micelles in solution, while more polymer chains remain free in solution. At pH 5, both the acrylic acid species and amine entities are mainly in their ionic form, unlike at pH 3 and 9, where one species or the other is much less charged. The shape of the neutron scattering curves, characteristic of core-shell morphologies, is similar for the three pH levels; nevertheless, it is less marked at pH 3 and 9 than at pH 5. At pH 5, the difference in intensity between the low q domain and the high q domain is higher and better marked, as expected for core−shell micelles with a well-defined interface between the core and the shell. The three curves could be fitted using the polymer micelle model, indicating a micellar structure even as the pH is changed, with the results of the fits given in Table 5. Nevertheless, when moving from a lower to a higher pH, a strong variation in the core radius, R, and radius of gyration of the P(OEGMEA) chains, R_g, was observed. Indeed, the core radius was determined as R = 4.3 ± 0.2 nm, 5.2 ± 0.3 nm, and 4.4 ± 1.3 nm, and the radius of gyration as R_g = 1.6 ± 0.2 nm, 1.8 ± 0.2 nm, and 0.6 ± 0.1 nm at pH = 3, 5, and 9, respectively. Let us note that the surprisingly low value of R_g at pH = 9 is accompanied by a similar decrease in the volume of one chain in the shell v_{shell} and is related to the very high polydispersity index at this pH, which prevents extracting a completely accurate value for the shell of the micelles. Indeed, the polydispersity in size (σ) varies from about 35% (at pH = 3 and 5) to about 74% (at pH = 9). The lower intensity associated with a large increase in the polydispersity in size confirms that at pH = 9, the system starts to lose its self-assembling properties, in agreement with the DLS data. This can be related to the value of the pH, which is close to the pK_a of Acyl urea.

3.4.2. Characterization of Ami. Pol.: Probing the Micellization Mechanisms as a Function of pH and Salinity. The pH sensitivity of this system was explored in more detail with the amidated copolymer Ami. Pol. 1, P(OEGMEA)$_{24}$-*b*-P((AA)$_{28}$-*s*-(Acyl urea)$_{17}$-*s*-(N-Boc)$_8$. The self-assembling properties are maintained after the addition of the N-Boc group (see Figure 6), and the pH-sensitive nature of the self-

https://doi.org/10.1021/acs.macromol.4c02884
Macromolecules 2025, 58, 5110−5134

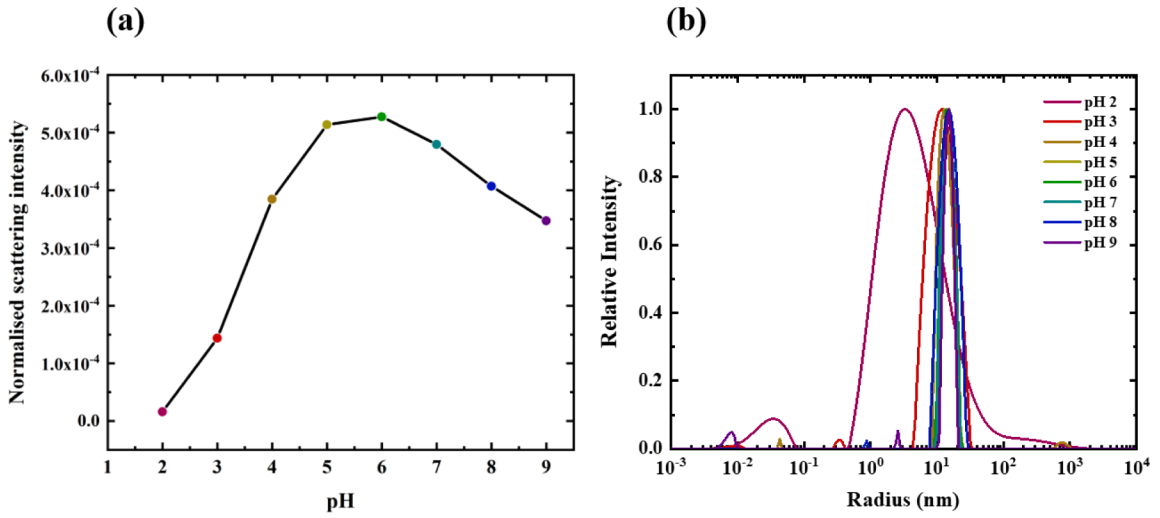

Figure 7. (a) Variation of the scattered light intensity of Ami. Pol. 1 suspensions normalized by the primary laser intensity as a function of pH (2−9) in H_2O (0.1 wt %) and (b) associated size distribution from the intensity time autocorrelation function $g_2(\tau)$ at a scattering angle of θ = 90 ° analyzed using CONTIN (associated correlograms are provided in Figure S8).

assembled structures was studied in detail using DLS while varying the pH between 2 and 9 (Figure 7).

First, the variation of the normalized scattered light intensity was studied as a function of pH (see Figure 7a). One can observe an increase in intensity with pH up to pH 5−6, followed by a decrease under alkaline conditions. This pH dependence of the self-assembly of the copolymer further suggests that electrostatic complexation between the negatively charged acrylate species and the positively charged *N*-Acyl urea groups is primarily responsible for micelle formation, similar to polyion complex micelles,[36,55,87] rather than an intrinsic amphiphilic property of the polymer. Such an amphiphilic property could also be expected from both the *N*-Boc-ethylenediamine and *N*-Acyl urea grafting on the copolymer,[53,88,89] as both the *tert*-butyl group in *N*-boc and *N*-Acyl urea species are known to exhibit moderate hydrophobicity. Indeed, the highest value of the scattered intensity is obtained at an intermediate pH range of 5−6, a range between the pK_a of the acrylic acid monomer (ca. 4.30)[90] and that of the amine in *N*-Acyl urea (ca. 9−10).[60,61] Moving away from this ideal pH range leads to the progressive dissociation of the micelles into individual polymer chains, resulting in a decrease in scattered intensity. Notably, the scattered intensity at pH = 2 is very weak, suggesting that at this pH, no micelles are formed in solution. This is further evidenced by studying the results from the CONTIN analysis of the DLS data at different pHs (Figure 7b). In a specific pH window between 4 and 9, particles with a monomodal size distribution and low polydispersity are observed, further confirming an optimal pH range for micellization around pH 5. As soon as one moves away from this pH range, the peaks widen, which may be due to multiple populations or high polydispersity. At pH = 5, the hydrodynamic radius obtained was similar to that of the activated copolymer (Act. Pol.), with an R_H of 14.6 ± 0.2 nm at the same pH (even though bulky *N*-Boc groups are grafted to the copolymer). The CONTIN analysis shows a narrower size distribution for the amidated copolymer (Figure 6a) compared to that of the activated copolymer (Figure 4a). This narrow size distribution could be attributed to the fact that the grafting of the *N*-Boc species reinforces the self-assembling behavior of the copolymers (through its hydrophobicity). As with the activated copolymer, the hydrodynamic radius R_H obtained by DLS was compared with the radius of gyration of micelles R_G obtained using the Guinier approximation on the SANS data at pH = 5 to characterize the shape of the species. This analysis again corresponds to a nonhomogeneous but spherical population, R_G/R_H = 0.63 ± 0.03 (Figure S9).

In order to further characterize the micelles, SANS measurements of Ami. Pol. 1 at 1 wt % in D_2O and pH ranging from 2 to 9 were performed (Figure 8). Once again,

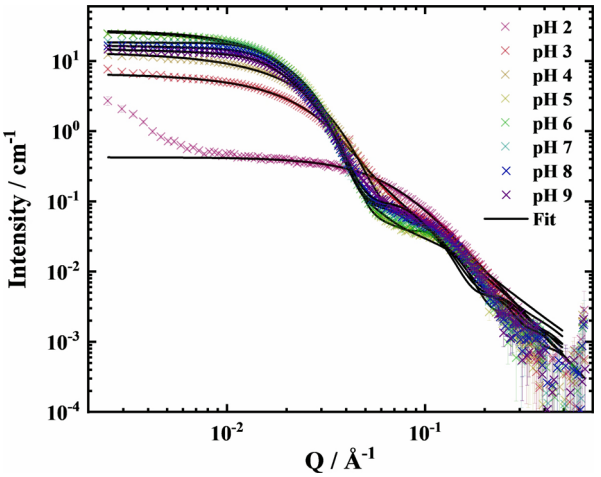

Figure 8. SANS patterns of Ami. Pol. 1 suspensions at 1 wt % and various pHs (2−9) in D_2O. In black, the fits were made using the polymer micelle model (pH 3−9) or the model of free polymer chains in solution (pH 2).

scattering curves from pH 3 to 9 were fitted with the polymer micelle model. At pH 5, the scattering curve for Ami. Pol. 1 is similar to that of Act. Pol. at the same pH, albeit with a slightly higher overall intensity at low q for the amidated copolymer micelles. From the fit of the sample at pH 5, the core radius R and chain gyration radius R_g were found to be 6.3 ± 0.1 nm and 3.3 ± 0.1 nm, respectively (with a polydispersity in size σ = 13 ± 2%). In the range of pH 3−9, the shape of the scattering curves remains about the same. However, the overall

https://doi.org/10.1021/acs.macromol.4c02884
Macromolecules 2025, 58, 5110−5134

intensity is notably lower at pH 3 and 4 than at pH 5, which could be due to a partial assembly in solution, as P(AA) is only partially charged at those pH values. According to the model, at pH = 3, the radius of the core R and the gyration radius R_g of the polymers in the shell were 3.5 ± 0.2 and 2.1 ± 0.1 nm, respectively, with a polydispersity in size σ = 55 ± 3%. For pH 4, the core radius R was 3.3 ± 0.2 nm, while R_g was found to be 3.6 ± 0.1 nm, with a polydispersity in size σ = 28 ± 5%. In pH 5−9, the shape and intensity are more constant and change less. Nevertheless, the addition of a structure factor is required to fit the data for pH 7−9 due to the appearance of a weak but notable correlation peak at q ca. 0.010 Å^{-1}, which was interestingly absent at pH 5 and 6. The fitting values obtained for the above pH levels are displayed in Table 5. At pH 2, the high intensity at the low to medium q-range disappears, proving the absence of well-defined micelles at this pH. Also, the decrease observed at ca. q = 0.1 Å^{-1} does not correspond as well to the second decrease from the micellar shell seen at the other pH levels. It was hence associated with a signal from free polymers in solution. Further, upon focusing on the low q region (0.004 < q < 0.008 Å^{-1}), the SANS pattern indicates an upturn suggesting interpolymeric interactions and, therefore, aggregation of polymers. Consequently, the curve was fitted using a free polymer chain model with a polymer radius of gyration R'_g = 2.7 ± 0.1 nm, which is in line with the size of the polymer chain. Let us note that at high q (0.1 < q < 0.4 Å^{-1}), the intensity follows a $q^{-\alpha}$ behavior, with α = 3.1 ± 0.1, in agreement with a copolymer presenting a comb-like block.

The prevailing effect of pH on the formation and dissociation of micelles from the modified copolymers (activated and amidated) concurs with the hypothesis that the self-assembly results from the electrostatic interactions between the unmodified acrylate groups and the tertiary amine entities of grafted *N*-Acyl urea, rather than from the mild hydrophobicity of *N*-Boc and *N*-Acyl urea. Indeed, the behavior of the modified micelles described here is similar to that of the well-studied polyion complex micelles; however, it surpasses them in their ability to self-assemble without the need for a complexation partner. To validate this hypothesis unambiguously, we studied the ζ-potential and the ionization coefficient of the acrylate groups of another amidated copolymer, Ami. Pol. 5, as a function of pH (Figure 9). The ionization coefficient, i.e., the ratio $COO^-/(COOH + COO^-)$ in the polymer, was calculated by a careful study of the COOH and COO^- bands monitored in ATR-FTIR between 1800 and 1500 cm^{-1} (see Figure S10). In acidic conditions, ζ-potential measurements give an overall positive charge of ca. + 10 mV, in agreement with the low ionization coefficient of the poly(acrylic acid) block (found at 0% at pH 2 and ca. 15% at pH 3), indicating the predominance of the positive charges of tertiary amines. With increasing pH values, the poly(acrylic acid) block in the copolymer is gradually deprotonated, resulting in a larger ionization coefficient and a decreasing ζ-potential. Interestingly, the isoelectric point of the macromolecule was detected by ζ-potential measurements for pH = 5−6, which corresponds to ionization coefficients of ca. 20 to 45%. NMR studies of Ami. Pol. 5 give conversion rates of 32% in *N*-Acyl urea pending groups and ca. 8% in *N*-Boc, leaving around 60% of acrylic acid functions on the polymer. From these values, we calculated a theoretical isoelectric point for this polymer at an ionization coefficient of 30%, which is indeed reached at pH = 5−6, corroborating the ζ-potential experimental data. In alkaline conditions, the ionization coefficient further increases, reaching ca. 80% at pH = 9, while the ζ-potential becomes strongly negative, as the negative charges from acrylates become predominant over the positive charges from tertiary amines. From the ionization coefficient curve, we could determine the apparent pK_a of the polyacid block in the copolymer at 6.4, in good agreement with the literature.[66] Although it was not possible to similarly determine the ionization coefficient of the tertiary amine, their known high pK_{aH} (around 9.76) suggests that positive charges should be present in the entire pH range probed. When compared with DLS and SANS studies, these results demonstrate that micellization occurs around pH = 3−4, once Ami. Pol. starts exhibiting negative charges by the partial ionization of the polyacid block that can interact with the positively charged tertiary amines. Further, the micellization optimum at ca. pH = 6, monitored in DLS and SANS, is consistent with the point of charge equivalence in the electrostatic balance of the polymer, as seen by the low value of the ζ-potential and its closeness to the theoretical isoelectric point.

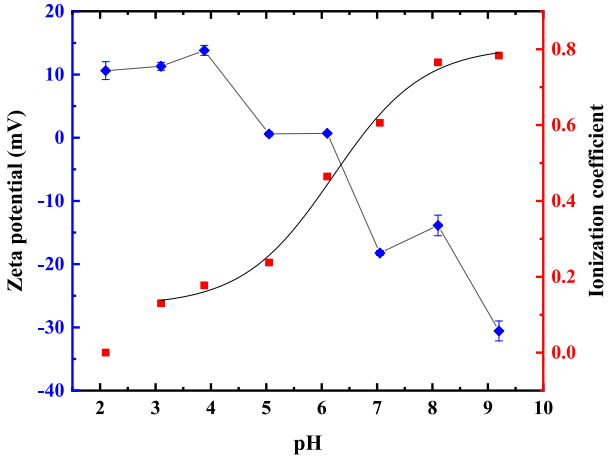

Figure 9. Comparison between the ζ-potential and the ionization coefficient $COO^-/(COOH + COO^-)$ in Ami. Pol. 5 as a function of pH. The lines are for guiding the eye only.

A micellization process that depends on electrostatic complexation should be sensitive to the ionic strength of the system, as the addition of salt can screen the charges present on the DHBC. We have therefore studied this phenomenon using DLS in Ami. Pol. 5 at pH 5 and different concentrations of NaCl, ranging from 0 to 1 M. Figure S11 presents the averaged scattered intensity as a function of the salt concentration and the associated correlation functions in intensity $g_2(\tau)$. The scattered intensity shows a clear decrease with increasing concentration, which is consistent with a decrease in the number of micelles in solution. Accordingly, the correlation function evolves from a signal of one well-defined population at 0 M to a signal from highly polydisperse systems at [NaCl] = 1 M, again aligning with the loss of micellization properties as the salt concentration increases.

When thoroughly compared, these results establish conclusively that micellization occurs due to electrostatic complexation as soon as the DHBC exhibits both positive and negative charges, even if the charges are not completely balanced within the polymer.

3.4.3. Characterization of Ami. Pol.: Probing the Effect of Concentration. The effect of concentration on the size and

https://doi.org/10.1021/acs.macromol.4c02884
Macromolecules 2025, 58, 5110−5134

shape of the self-assembling species was studied using Ami. Pol. 1 suspensions at pH = 5 in D_2O (1−5 wt %), measured by SANS. As shown in Figure 10, the absolute scattering intensity

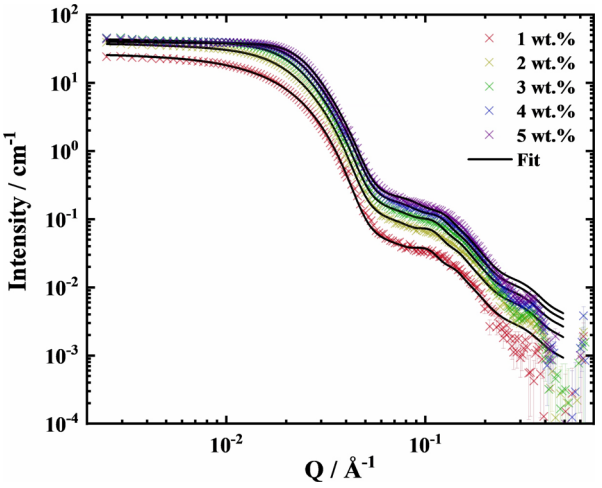

Figure 10. SANS patterns for Ami. Pol. 1 micelles made at pH = 5 in D_2O and at different concentrations (1−5 wt %).

of the solutions increases with concentration, as expected due to the increase in the number of scattering objects. At 1 wt %, no characteristics of intermicellar interaction were observed, and the data could be fitted using only the form factor of polymer micelles ($S(q) = 1$). However, by increasing the copolymer concentration from 2 wt % to 5 wt %, a structure factor peak at q ca. 0.02 Å^{-1} becomes increasingly more pronounced, indicating the emergence of intermicellar interactions, modeled with a hard sphere structure factor (see Materials and Methods).

The core radius of the micelles R was found to decrease with concentration (from 6.3 ± 0.1 nm at 1 wt % to 4.9 ± 0.1 nm at 5 wt %), while the gyration radius of the chains in the shell R_g remains roughly constant at ca. 3.3 nm. This phenomenon has been observed previously for micelles formed by electrostatic interaction between the charged block of a DHBC and an oppositely charged micellization partner, as increasing the concentration results in less water in the micelle core, thereby reducing its size.[74] This suggests that these self-assembled micelles, also formed by electrostatic complexation between positively and negatively charged units present within the same block, follow the same trend. Hence, one could expect the micelle core to be rich in water, as was previously observed with PIC micelles, reaching in some cases up to 50 vol % of the core.[74] It should be noted that in our model, the SLD of the core was calculated while neglecting the presence of water. Although this is likely incorrect, it would have little influence on the other parameters of the fits, except for the overall scaling factor (related to the volume fraction of particles), which would be affected by an error in SLDs. As SLDs cannot be accurately extracted with a single contrast, the actual value of the scale is not discussed here, but only the trends are considered . Notably, with increasing concentration, the scale factor increases almost linearly, which is expected because it would follow the increase in volume fraction. More surprisingly, the volume of the shell v_{shell} decreases with concentration, which may be related to a reduction in the water content in the shell.[74] As for the intermicelle interactions, they were modeled using the hard-sphere structure factor, which is the simplest possible model. The hard-sphere radius of interactions R_{HS} decreases as the concentration increases (from 15.1 ± 0.3 nm at 2 wt % to 12.5 ± 0.1 nm at 5 wt %), as expected. By defining $R_{tot} = R + 2R_g$ the total radius of one micelle, it is interesting to study the variation of $\frac{R_{HS}}{R_{tot}}$ with concentration. $\frac{R_{HS}}{R_{tot}}$ decreases from 1.19 ± 0.03 at 2 wt % to 1.09 ± 0.02 at 5 wt %, but remains >1, indicating that micelles are not yet in close contact or interpenetrating. On the other hand, the volume fraction of interacting particles φ_{HS} increases almost monotonously with concentration, as expected. All of the parameters from the fits are provided in Table 6.

3.4.4. Characterization of Ami. Pol.: Comparison Between Ami. Pol. 1−4. The self-assembling nature of the P(OEGMEA)-*b*-P(AA-*s*-(Acyl urea)-*s*-(*N*-Boc)) copolymer was further substantiated using multiple batches of the amidated copolymer (Ami. Pol. 1 to 4) comprising different degrees of *N*-Boc grafting (up to 34% of the block units). Figure S12 depicts the NMR pattern of the *N*-Boc-incorporated copolymers, and Figure S13 shows the SANS plot of the above polymers at 1 wt % in D_2O, pH 5. The shape and scattering intensity of the different batches did not evolve drastically (see fitting parameters in Table S5) proving the consistency of the results discussed above, even at a higher amount of *N*-Boc grafting. An interesting feature can nevertheless be noted: Figure S13 shows that the self-assembly process of the amidated copolymers is favored when the fractions of *N*-Acyl urea are the highest, as evidenced by the highest intensity at low q values and the much more marked interface suggested by the higher slope at q ca. 0.04 Å^{-1} when the fraction of Acyl urea is higher. These results highlight that micellization is favored when the ratio between negative charges (from the remaining acrylate groups) and positive charges (from *N*-Acyl urea) is closer to one.

Table 6. Parameters Obtained from the SANS Data Fitting of Micelles from Ami. Pol. 1 at Various Concentrations (1−5 wt %) Using the Model of Polymer Micelles[a]

						Structural factor	
Concentration	Scale	Radius, R, nm	Radius of gyration, R_g, nm	Volume of shell v_{shell}, nm^3	Polydispresity, %	Volume fraction, %	Hard sphere radius, nm
1	0.14×10^{-6} (0.01×10^{-6})	6.3 (0.1)	3.3 (0.1)	0.72×10^{2} (0.01×10^{2})	13 (2)	----	-----
2	0.29×10^{-6} (0.01×10^{-6})	5.9 (0.1)	3.4 (0.1)	0.71×10^{2} (0.01×10^{2})	14 (1)	3 (1)	15.1 (0.3)
3	0.42×10^{-6} (0.02×10^{-6})	5.7 (0.1)	3.3 (0.1)	0.67×10^{2} (0.01×10^{2})	15 (2)	5 (1)	14.0 (0.2)
4	0.58×10^{-6} (0.02×10^{-6})	5.3 (0.1)	3.3 (0.1)	0.61×10^{2} (0.01×10^{2})	16 (2)	8 (1)	13.1 (0.1)
5	0.73×10^{-6} (0.02×10^{-6})	4.9 (0.1)	3.3 (0.1)	0.58×10^{2} (0.01×10^{2})	18 (2)	10 (1)	12.5 (0.1)

[a]For each parameter, the standard error is provided between parentheses.

https://doi.org/10.1021/acs.macromol.4c02884
Macromolecules 2025, 58, 5110−5134

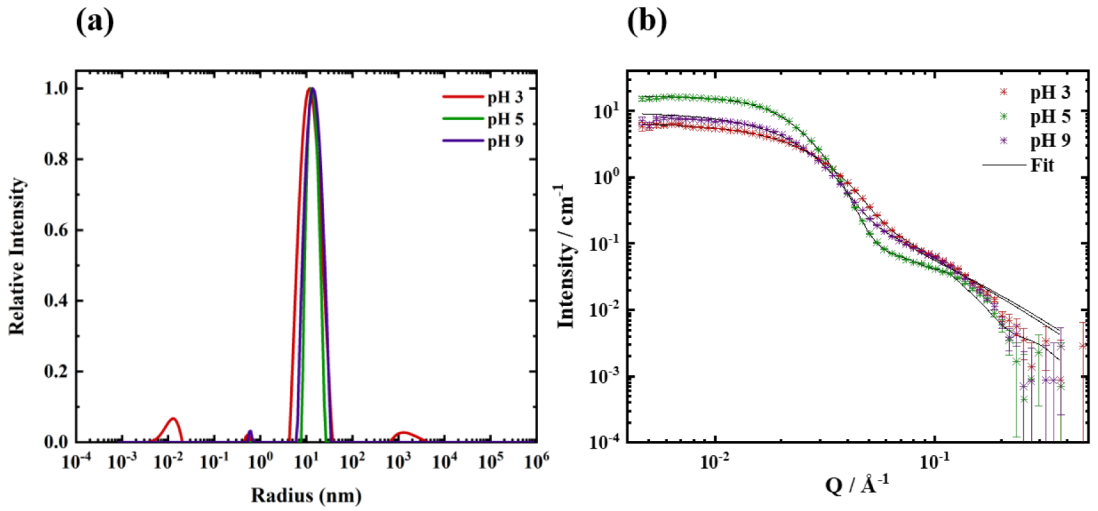

Figure 11. (a) Distribution of size from intensity-time autocorrelation functions $g_2(\tau)$ studied at a scattering angle of $\theta = 90°$ for De. Pol. 1 micelles at 0.1 wt % in H_2O and various pHs using the CONTIN method (associated correlograms are provided in Figure S8) and (b) corresponding SANS curves at 1 wt % in D_2O. In (b), the fit made using the polymer micelle model is given as black lines. The pH studied are pH = 3 (red), 5 (green), and 9 (purple).

3.4.5. Characterization of De. Pol.: Influence of Primary Amines on the Self-Assemblies. Light and small-angle neutron scattering experiments were conducted on De. Pol. 1 suspensions to investigate the effect of deprotection on the self-assembling properties of the copolymer. DLS results indicate matching features for both samples at pH = 5, before and after deprotection (see Figure 6a for the sample before deprotection and Figure S14a for the sample after deprotection). The pH behavior is also similar for protected and deprotected samples (see Figures 7b and 11a). Notably, both samples at pH = 5 exhibit similar hydrodynamic radii, with R_H = 14.6 ± 0.2 nm before deprotection and R_H = 13.8 ± 0.3 nm after deprotection (based on the CONTIN analysis). Additionally, both samples display the same pH response, with an optimal range at 5−6. Similarly, SANS patterns before (see Figure 6b) and after deprotection (Figures 11b and S14b) show the same features, with a plateau at small angles followed by a marked intensity decrease at ca. q = 0.02 $Å^{-1}$ corresponding to the size of the micelles, and a second decrease at ca. q = 0.1 $Å^{-1}$ followed by a slope $q^{-\alpha} \geq q^{-3}$ (α = 3.0, 3.2, and 3.0 at pH = 3, 5, and 9, respectively, for the deprotected sample) associated with the shell of P(OEGMEA) comb-like chains of the micelles. The highly similar results obtained before and after deprotection are consistent with the low fraction of protected *N*-Boc groups in the functional block for this particular polymer (8 units in a 53-unit block): neither the overall size (R_H), the shape (spherical), nor the pH dependence of the micelle objects seems significantly affected by the deprotection step. The self-association behavior observed is likely primarily due to the electrostatic complexation between the Acyl urea−amine groups and the acrylate groups, which are present in more comparable amounts.

Nonetheless, overlapping SANS patterns of the polymer before and after deprotection measured at pH = 5 (see Figure S15) allows one to observe some subtle differences, notably the emergence of a very weak correlation peak at ca. q = 0.012 $Å^{-1}$ after deprotection. The fit of the data at pH = 5 for De. Pol. 1 was carried out using the polymer micelle model, taking into account the structure factor, and its results were compared with the conclusions from the corresponding amidated copolymer before deprotection (see Ami. Pol. 1 and De. Pol. 1 at pH = 5 in Table 5).

Upon fitting, a drop in core radius R from 6.3 ± 0.1 nm to 5.3 ± 0.1 nm was observed when transitioning from the protected to the deprotected sample, which we attribute to the removal of bulky *N*-Boc groups from the protected copolymer. The radius of gyration of the polymer chains in the shell R_g remained nearly unchanged in both cases (3.3 ± 0.1 and 3.5 ± 0.1 nm, respectively), and the polydispersity was also found to be within the same range (13 ± 2% and 17 ± 1%, respectively). The weakly emerged correlation peak in the deprotected sample indicates developing intermicellar interactions and has been modeled using a hard sphere structural factor, yielding a volume fraction of 5 ± 1% and a hard sphere radius of 15.0 ± 0.2 nm. The emergence of intermicellar interactions could suggest the formation of more micelles in the deprotected sample compared to its precursor (in agreement with the increase in scale factor (see Table 5) and may be related to changes in the charge balance and hydrophobicity within the micelle core due to the removal of *N*-Boc species. Notably, the deprotection of the copolymer introduces more positively charged species into the core, which may facilitate the formation of well-defined micelles.

To conclude, we have shown that it is possible to perform a postsynthesis modification using the EDC/NHS activation route followed by *N*-Boc-ethylenediamine, and with this method, modify a P(OEGMEA)-*b*-P(AA) DHBC by grafting *N*-Acyl urea groups and *N*-Boc-ethylenediamine. We have observed that modifying the conditions of activation and amidation, notably their pH, influences the amount of both functional groups in the amidated copolymer. Notably, by working at pH 8 for both the activation and amidation, a total amount of ca. 34% of *N*-Boc-ethylenediamine species can be grafted to the polymer. We demonstrated that the addition of *N*-Acyl urea groups imparts self-assembling properties to the polymer, allowing it to form well-defined spherical micelles in suspension. pH variation studies, combined with salt concentration studies, evidenced that electrostatic complexation bonding between N-Acyl urea and acrylate groups of the DHBC was responsible for these self-assembling properties,

https://doi.org/10.1021/acs.macromol.4c02884
Macromolecules 2025, 58, 5110−5134

while further modification with *N*-Boc-ethylenediamine shows that additional functional groups can be added to the DHBC. We also verified that the deprotection step, which is mandatory to remove the *tert*-butyl group from the *N*-Boc-ethylenediamine, does not damage the DHBC and that the self-assembling properties are maintained after deprotection. The final DHBC, P(OEGMEA)-*b*-P(AA-*s*-(Acyl urea)-*s*-(AA/NH_2)), thus displays acrylate groups, primary amines, and tertiary amines—three different functional groups that could be transferred to a functional mesoporous material, following procedures established for materials templated with PIC micelles,[37,91] for example, for removing a wide range of pollutants in wastewater. The amount of primary amines (8 to 34%, depending on the amidation conditions) could be improved by further optimization of both activation and amidation protocols. Finally, the amidation procedure could be adapted to other nucleophilic amine-containing molecules to introduce additional functionalities to the DHBC.

4. CONCLUSION

In the present study, the self-assembly behavior of the double hydrophilic block copolymer, P(OEGMEA)-*b*-P(AA) after functionalization by partial amidation in an aqueous medium, has been studied in detail. P(OEGMEA)-*b*-P(AA) synthesized by RAFT polymerization using OEGMEA and AA as the precursors, was initially modified using EDC/NHS to derive an activated P(OEGMEA)-*b*-P(AA-*s*-(AA-NHS)-*s*-(Acyl urea)) copolymer that contains *N*-Acyl urea groups formed by the rearrangement of *O*-Acyl urea esters. This activated DHBC can self-assemble into well-defined micelles at controlled pH. The activated polymer was then transformed using *N*-Boc-ethylenediamine to yield the amidated copolymer, P(OEGMEA)-*b*-P(AA-*s*-(Acyl urea)-*s*-(*N*-Boc)), grafted with protected primary amine species while retaining its self-assembling properties. The parent copolymer, P(OEGMEA)-*b*-P(AA), was characterized using ^{1}H NMR to determine the number of units in each block along with the conversion rate, while the modified macromolecules (activated and amidated copolymers) obtained were studied using both NMR and elemental analysis to confirm the degree of modifications.

The self-assembling properties of both the activated and amidated copolymers were investigated using light and neutron scattering. The pH sensitivity of the self-assembling structures was studied through light scattering and further complemented by neutron experiments and ζ-potential measurements, with the pH varied between 2 and 9. For both activated and amidated polymers, well-defined core−shell spherical micelles were obtained over a wide range of pH (5−9, with an optimum at pH = 5−7), with the modified acrylic acid ionic block forming the core and P(OEGMEA) building the shell, as inferred from the SANS experiments conducted. However, moving away from this optimal pH range led to the progressive dissociation of the self-assembled structures. All the data for micellar suspensions obtained by SANS were fitted using a polymer micelle model, and a structure factor based on a hard-sphere model was applied when necessary. Specific information, including the core radius R and the gyration radius R_g of the P(OEGMEA) polymer chains forming the shell of the micelles, was collected from the neutron data. Additionally, we observed the effect of concentration in the amidated copolymer (Ami. Pol. 1) at pH 5 using SANS, confirming that increasing the concentration induced the rise of intermicelle interactions, which could be effectively modeled using a hard-sphere structure factor.

The induced self-assembling character of the polymers is expected mainly through complexation, deriving from the positively charged tertiary amine species in the *N*-Acyl urea chain and the negatively charged remaining acrylate functions, as confirmed by the pH- and salt-susceptible nature of the micelles. Notably, the gradual loss of micellization properties at pH < 5, associated with a gradual loss of the ionization coefficient of the acrylate groups, is well explained by the uncharged nature of the acrylic acid groups at these pH levels. A similar trend seems to emerge toward pH = 9, due to the gradual loss of the positive charges of the tertiary amine. Nonetheless, studies at higher pH (≥10) were not performed to avoid possible degradation of the P(OEGMEA) block. Micellization can also be controlled by the addition of salt; DLS measurements at various salt concentrations showed a gradual loss of the micelles due to charge screening. The mild hydrophobicity of the *tert*-butyl group and the *N*-Acyl urea added to the polymer seem to have only a minor impact on the self-assembling character of the micelle.

Acid hydrolysis of an amidated copolymer using TCA at pH = 1.75 removes the *tert*-butyl group from the *N*-Boc functionality of the copolymer and yields the final deprotected structure, P(OEGMEA)-*b*-P(AA-*s*-(Acyl urea)-*s*-(AA/NH_2)) featuring both primary and tertiary amines as pendant functions in the ionic block of the copolymer. This structure holds promise for applications in diverse domains, including separation and purification.[92−94] TCA, as a mild acid, is preferred over HCl or trifluoroacetic acid because it selectively removes the *tert*-butyl group of the *N*-Boc while preserving the esters in the P(OEGMEA) block. Characterization of the copolymer using NMR, EA, and scattering techniques confirms efficient deprotection while maintaining its self-assembling properties. Consequently, new DHBC polymers composed of a neutral comb-type block and a multifunctional ionic block, which simultaneously display anionic and cationic functions in similar amounts across a wide pH range, were successfully synthesized. Their self-assembly behavior results in the formation of unique electrostatically driven polyion complex micelles derived from a single polymer, which can be dissociated in acidic conditions when acrylate functions are neutralized.

■ ASSOCIATED CONTENT

Supporting Information

The Supporting Information is available free of charge at https://pubs.acs.org/doi/10.1021/acs.macromol.4c02884.

^{1}H NMR spectra of the parent copolymer and modified samples; composition details of activated, amidated and deprotected samples through elemental analysis; static and dynamic light scattering data along with neutron scattering data of specific samples; fitting parameters used for specific samples in SANS; comparing methods of deprotection; Infrared analysis of copolymers at different pH, and peak deconvolution in the carbonyl region (PDF)

■ AUTHOR INFORMATION

Corresponding Authors

Gaulthier Rydzek − *Institut Charles Gerhardt, UMR 5253, CNRS-ENSCM-UM, University of Montpellier, Montpellier*

https://doi.org/10.1021/acs.macromol.4c02884
Macromolecules 2025, 58, 5110−5134

Cedex 5 F-34295, France; orcid.org/0000-0002-2901-3441; Email: gaulthier.rydzek@umontpellier.fr

Julien Schmitt − *Institut Charles Gerhardt, UMR 5253, CNRS-ENSCM-UM, University of Montpellier, Montpellier Cedex 5 F-34295, France; LSFC − Laboratoire de Synthèse et Fonctionnalisation des Céramiques, UMR 3080 CNRS/Saint-Gobain CREE, Saint-Gobain Research Provence, Cavaillon 84300, France;* orcid.org/0000-0002-3452-6655; Email: julien.schmitt@umontpellier.fr

Authors

Ananthapadmanabhan Unnikrishnan − *Institut Laue − Langevin, DS/LSS Group, Grenoble Cedex 9 38042, France; Institut Charles Gerhardt, UMR 5253, CNRS-ENSCM-UM, University of Montpellier, Montpellier Cedex 5 F-34295, France*

Mateus Garcia Rodolfo − *Institut Charles Gerhardt, UMR 5253, CNRS-ENSCM-UM, University of Montpellier, Montpellier Cedex 5 F-34295, France;* orcid.org/0009-0009-9795-8760

Najet Mahmoudi − *ISIS Neutron and Muon Source, Science and Technology Facilities Council, Rutherford Appleton Laboratory, Didcot OX11 0QX, United Kingdom*

Ralf Schweins − *Institut Laue − Langevin, DS/LSS Group, Grenoble Cedex 9 38042, France;* orcid.org/0000-0001-8078-2089

Corine Gérardin − *Institut Charles Gerhardt, UMR 5253, CNRS-ENSCM-UM, University of Montpellier, Montpellier Cedex 5 F-34295, France;* orcid.org/0000-0002-6590-8103

Complete contact information is available at: https://pubs.acs.org/10.1021/acs.macromol.4c02884

Notes

The authors declare no competing financial interest.

■ ACKNOWLEDGMENTS

The authors express their sincere gratitude to the Physical Measurement Laboratory (Chemical Analysis Platform) at Université de Montpellier, France, for supporting the NMR and elemental analysis. Additionally, the authors are grateful to the Partnership for Soft Condensed Matter (PSCM) facilities at Grenoble, France, for facilitating all preliminary sample characterizations. The authors warmly thank Jan Skov Pedersen, who designed the Fortran software for SANS data analysis, which was modified by the authors to fit polymer micelles. This project has received funding from the European Union's Horizon 2020 research and innovation program under the Marie Skłodowska-Curie grant agreement No. 847439, through the InnovaXN scheme (Project XN2020-ILL30). All the authors thankfully acknowledge the beam times allotted by Institut Laue-Langevin (D22) and ISIS Neutron and Muon Source (Larmor, 10.5286/ISIS.E.RB2320268-2 and Sans2d, 10.5286/ISIS.E.RB2320268-1). This work benefited from the use of the SasView application, originally developed under NSF award DMR-0520547. SasView contains code developed with funding from the European Union's Horizon 2020 research and innovation program under the SINE2020 project, grant agreement No. 654000.

■ REFERENCES

(1) Lu, Y.; Lin, J.; Wang, L.; Zhang, L.; Cai, C. Self-Assembly of Copolymer Micelles: Higher-Level Assembly for Constructing Hierarchical Structure. *Chem. Rev.* **2020**, *120* (9), 4111−4140.

(2) Boles, M. A.; Engel, M.; Talapin, D. V. Self-Assembly of Colloidal Nanocrystals: From Intricate Structures to Functional Materials. *Chem. Rev.* **2016**, *116* (18), 11220−11289.

(3) Kötz, J.; Kosmella, S.; Beitz, T. Self-Assembled Polyelectrolyte Systems. *Prog. Polym. Sci.* **2001**, *26* (8), 1199−1232.

(4) *Amphiphilic Block Copolymers Self-Assembly and Applications*; Alexandridis, P.; Lindman, B., Eds.; Elsevier, 2000. DOI: .

(5) Mai, Y.; Eisenberg, A. Self-Assembly of Block Copolymers. *Chem. Soc. Rev.* **2012**, *41* (18), 5969.

(6) Malmsten, M.; Lindman, B. Self-Assembly in Aqueous Block Copolymer Solutions. *Macromolecules* **1992**, *25* (20), 5440−5445.

(7) Al Nakeeb, N.; Willersinn, J.; Schmidt, B. V. K. J. Self-Assembly Behavior and Biocompatible Cross-Linking of Double Hydrophilic Linear-Brush Block Copolymers. *Biomacromolecules* **2017**, *18* (11), 3695−3705.

(8) Casse, O.; Shkilnyy, A.; Linders, J.; Mayer, C.; Häussinger, D.; Völkel, A.; Thünemann, A. F.; Dimova, R.; Cölfen, H.; Meier, W.; Schlaad, H.; Taubert, A. Solution Behavior of Double-Hydrophilic Block Copolymers in Dilute Aqueous Solution. *Macromolecules* **2012**, *45* (11), 4772−4777.

(9) Boudier, A.; Aubert-Pouëssel, A.; Gérardin, C.; Devoisselle, J.-M.; Bégu, S. pH-Sensitive Double-Hydrophilic Block Copolymer Micelles for Biological Applications. *Int. J. Pharm.* **2009**, *379* (2), 212−217.

(10) Bathfield, M.; Warnant, J.; Gérardin, C.; Lacroix-Desmazes, P. Asymmetric Neutral, Cationic and Anionic PEO-Based Double-Hydrophilic Block Copolymers (DHBCs): Synthesis and Reversible Micellization Triggered by Temperature or pH. *Polym. Chem.* **2015**, *6* (8), 1339−1349.

(11) Khimani, M.; Patel, H.; Patel, V.; Parekh, P.; Vekariya, R. L. Self-Assembly of Stimuli-Responsive Block Copolymers in Aqueous Solutions: An Overview. *Polym. Bull.* **2020**, *77* (11), 5783−5810.

(12) Hoogenboom, R.; Rogers, S.; Can, A.; Becer, C. R.; Guerrero-Sanchez, C.; Wouters, D.; Hoeppener, S.; Schubert, U. S. Self-Assembly of Double Hydrophobic Block Copolymers in Water−Ethanol Mixtures: From Micelles to Thermoresponsive Micellar Gels. *Chem. Commun.* **2009**, No. 37, 5582.

(13) RodrÍguez-Hernández, J.; Lecommandoux, S. Reversible Inside−Out Micellization of pH-Responsive and Water-Soluble Vesicles Based on Polypeptide Diblock Copolymers. *J. Am. Chem. Soc.* **2005**, *127* (7), 2026−2027.

(14) Arotçaréna, M.; Heise, B.; Ishaya, S.; Laschewsky, A. Switching the Inside and the Outside of Aggregates of Water-Soluble Block Copolymers with Double Thermoresponsivity. *J. Am. Chem. Soc.* **2002**, *124* (14), 3787−3793.

(15) Nabiyan, A.; Max, J. B.; Schacher, F. H. Double Hydrophilic Copolymers − Synthetic Approaches, Architectural Variety, and Current Application Fields. *Chem. Soc. Rev.* **2022**, *51* (3), 995−1044.

(16) Zhuang, J.; Gordon, M. R.; Ventura, J.; Li, L.; Thayumanavan, S. Multi-Stimuli Responsive Macromolecules and Their Assemblies. *Chem. Soc. Rev.* **2013**, *42* (17), 7421.

(17) Cheng, R.; Meng, F.; Deng, C.; Klok, H.-A.; Zhong, Z. Dual and Multi-Stimuli Responsive Polymeric Nanoparticles for Programmed Site-Specific Drug Delivery. *Biomaterials* **2013**, *34* (14), 3647−3657.

(18) Karimi, M.; Sahandi Zangabad, P.; Ghasemi, A.; Amiri, M.; Bahrami, M.; Malekzad, H.; Ghahramanzadeh Asl, H.; Mahdieh, Z.; Bozorgomid, M.; Ghasemi, A.; Rahmani Taji Boyuk, M. R.; Hamblin, M. R. Temperature-Responsive Smart Nanocarriers for Delivery Of Therapeutic Agents: Applications and Recent Advances. *ACS Appl. Mater. Interfaces* **2016**, *8* (33), 21107−21133.

(19) El Jundi, A.; Buwalda, S. J.; Bakkour, Y.; Garric, X.; Nottelet, B. Double Hydrophilic Block Copolymers Self-Assemblies in Biomedical Applications. *Adv. Colloid Interface Sci.* **2020**, *283*, 102213.

(20) Felber, A. E.; Dufresne, M.-H.; Leroux, J.-C. pH-Sensitive Vesicles, Polymeric Micelles, and Nanospheres Prepared with Polycarboxylates. *Adv. Drug Delivery Rev.* **2012**, *64* (11), 979−992.
(21) Ge, Z.; Xie, D.; Chen, D.; Jiang, X.; Zhang, Y.; Liu, H.; Liu, S. Stimuli-Responsive Double Hydrophilic Block Copolymer Micelles with Switchable Catalytic Activity. *Macromolecules* **2007**, *40* (10), 3538−3546.
(22) Warnant, J.; Marcotte, N.; Reboul, J.; Layrac, G.; Aqil, A.; Jerôme, C.; Lerner, D. A.; Gérardin, C. Physicochemical Properties of pH-Controlled Polyion Complex (PIC) Micelles of Poly(Acrylic Acid)-Based Double Hydrophilic Block Copolymers and Various Polyamines. *Anal. Bioanal. Chem.* **2012**, *403* (5), 1395−1404.
(23) Zhang, X. A.; Chen, M. R.; Zhao, H.; Gao, Y.; Wei, Q.; Zhang, S.; Qin, A.; Sun, J. Z.; Tang, B. Z. A Facile Synthetic Route to Functional Poly(Phenylacetylene)s with Tunable Structures and Properties. *Macromolecules* **2011**, *44* (17), 6724−6737.
(24) Zhu, Z.; Pan, X.; Zhang, W.; Li, H.; Wang, W.; He, Y. Amphiphilic Block Copolymer with Diazonium Salt Pendant Groups: Synthesis, Self-Assembly and Post-Modification. *React. Funct. Polym.* **2022**, *179*, 105377.
(25) Sanson, N.; Bouyer, F.; Destarac, M.; In, M.; Gérardin, C. Hybrid Polyion Complex Micelles Formed from Double Hydrophilic Block Copolymers and Multivalent Metal Ions: Size Control and Nanostructure. *Langmuir* **2012**, *28* (8), 3773−3782.
(26) Gineste, S.; Lonetti, B.; Yon, M.; Giermanska, J.; Di Cola, E.; Sztucki, M.; Coppel, Y.; Mingotaud, A.-F.; Chapel, J.-P.; Marty, J.-D.; Mingotaud, C. Hybrid Polymeric Micelles Stabilized by Gallium Ions: Structural Investigation. *J. Colloid Interface Sci.* **2022**, *609*, 698−706.
(27) Layrac, G.; Destarac, M.; Gérardin, C.; Tichit, D. Highly Stable Layered Double Hydroxide Colloids: A Direct Aqueous Synthesis Route from Hybrid Polyion Complex Micelles. *Langmuir* **2014**, *30* (32), 9663−9671.
(28) Bouyer, F.; Sanson, N.; Destarac, M.; Gérardin, C. Hydrophilic Block Copolymer-Directed Growth of Lanthanum Hydroxide Nanoparticles. *New J. Chem.* **2006**, *30* (3), 399.
(29) Tarasov, K.; Houssein, D.; Destarac, M.; Marcotte, N.; Gérardin, C.; Tichit, D. Stable Aqueous Colloids of ZnS Quantum Dots Prepared Using Double Hydrophilic Block Copolymers. *New J. Chem.* **2013**, *37* (2), 508−514.
(30) Antonietti, M.; Breulmann, M.; Göltner, C. G.; Cölfen, H.; Wong, K. K. W.; Walsh, D.; Mann, S. Inorganic/Organic Mesostructures with Complex Architectures: Precipitation of Calcium Phosphate in the Presence of Double-Hydrophilic Block Copolymers. *Chem.-eur. J.* **1998**, *4* (12), 2493−2500.
(31) Bronstein, L. M.; Chernyshov, D. M.; Timofeeva, G. I.; Dubrovina, L. V.; Valetsky, P. M.; Obolonkova, E. S.; Khokhlov, A. R. Interaction of Polystyrene- *Block* -Poly(Ethylene Oxide) Micelles with Cationic Surfactant in Aqueous Solutions. Metal Colloid Formation in Hybrid Systems. *Langmuir* **2000**, *16* (8), 3626−3632.
(32) Bathfield, M.; Reboul, J.; Cacciaguerra, T.; Lacroix-Desmazes, P.; Gérardin, C. Thermosensitive and Drug-Loaded Ordered Mesoporous Silica: A Direct and Effective Synthesis Using PEO- *b* -PNIPAM Block Copolymers. *Chem. Mater.* **2016**, *28* (10), 3374−3384.
(33) Baccile, N.; Reboul, J.; Blanc, B.; Coq, B.; Lacroix-Desmazes, P.; In, M.; Gérardin, C. Ecodesign of Ordered Mesoporous Materials Obtained with Switchable Micellar Assemblies. *Angew. Chem., Int. Ed.* **2008**, *120* (44), 8561−8565.
(34) Molina, E.; Mathonnat, M.; Richard, J.; Lacroix-Desmazes, P.; In, M.; Dieudonné, P.; Cacciaguerra, T.; Gérardin, C.; Marcotte, N. pH-Mediated Control over the Mesostructure of Ordered Mesoporous Materials Templated by Polyion Complex Micelles. *Beilstein J. Nanotechnol.* **2019**, *10*, 144−156.
(35) Richard, J.; Phimphachanh, A.; Jamet-Fournier, A.; Cacciaguerra, T.; Dieudonné-George, P.; Cot, D.; Destarac, M.; Lacroix-Desmazes, P.; In, M.; Marcotte, N.; Gérardin, C. Dual Control of External Surface and Internal Pore Structure of Small Ordered Mesoporous Silica Particles Directed by Mixed Polyion Complex Micelles. *Microporous Mesoporous Mater.* **2022**, *338*, 111915.
(36) Houssein, D.; Warnant, J.; Molina, E.; Cacciaguerra, T.; Gérardin, C.; Marcotte, N. Mesoporous Silica Templated by Polyion Complex Micelles: A Versatile Approach for Controlling the Mesostructure. *Microporous Mesoporous Mater.* **2017**, *239*, 244−252.
(37) Richard, J.; Phimphachanh, A.; Schneider, J.; Nandi, S.; Laurent, E.; Lacroix-Desmazes, P.; Trens, P.; Devautour-Vinot, S.; Marcotte, N.; Gérardin, C. Integrated Process for Structuring and Functionalizing Ordered Mesoporous Silica to Achieve Superprotonic Conductivity. *Chem. Mater.* **2022**, *34* (17), 7828−7836.
(38) Gauthier, M. A.; Gibson, M. I.; Klok, H. Synthesis of Functional Polymers by Post-Polymerization Modification. *Angew. Chem. Int. Ed* **2009**, *48* (1), 48−58.
(39) Liu, X.; Hu, D.; Jiang, Z.; Zhuang, J.; Xu, Y.; Guo, X.; Thayumanavan, S. Multi-Stimuli-Responsive Amphiphilic Assemblies through Simple Postpolymerization Modifications. *Macromolecules* **2016**, *49* (17), 6186−6192.
(40) Zhong, Y.; Zeberl, B. J.; Wang, X.; Luo, J. Combinatorial Approaches in Post-Polymerization Modification for Rational Development of Therapeutic Delivery Systems. *Acta Biomater* **2018**, *73*, 21−37.
(41) Riemer, S.; Prévost, S.; Dzionara, M.; Gasser, U.; Gradzielski, M. Hydrophobically Modified Polyacrylates (hmPAAs) with Long Alkyl Chains − Self-Assembly in Aqueous Solution. *Polymer* **2017**, *128*, 78−86.
(42) McCormick, C. L.; Middleton, J. C.; Cummins, D. F. Water-Soluble Copolymers. 37. Synthesis and Characterization of Responsive Hydrophobically Modified Polyelectrolytes. *Macromolecules* **1992**, *25* (4), 1201−1206.
(43) Sam, S.; Touahir, L.; Salvador Andresa, J.; Allongue, P.; Chazalviel, J.-N.; Gouget-Laemmel, A. C.; Henry De Villeneuve, C.; Moraillon, A.; Ozanam, F.; Gabouze, N.; Djebbar, S. Semiquantitative Study of the EDC/NHS Activation of Acid Terminal Groups at Modified Porous Silicon Surfaces. *Langmuir* **2010**, *26* (2), 809−814.
(44) Oh, E. J.; Park, K.; Kim, K. S.; Kim, J.; Yang, J.-A.; Kong, J.-H.; Lee, M. Y.; Hoffman, A. S.; Hahn, S. K. Target Specific and Long-Acting Delivery of Protein, Peptide, and Nucleotide Therapeutics Using Hyaluronic Acid Derivatives. *J. Controlled Release* **2010**, *141* (1), 2−12.
(45) Martin, J.; Desfoux, A.; Martinez, J.; Amblard, M.; Mehdi, A.; Vezenkov, L.; Subra, G. Bottom-up Strategies for the Synthesis of Peptide-Based Polymers. *Prog. Polym. Sci.* **2021**, *115*, 101377.
(46) Pedone, E.; Li, X.; Koseva, N.; Alpar, O.; Brocchini, S. An Information Rich Biomedical Polymer Library. *J. Mater. Chem.* **2003**, *13* (11), 2825−2837.
(47) Ferruti, P.; Bettelli, A.; Feré, A. High Polymers of Acrylic and Methacrylic Esters of N-Hydroxysuccinimide as Polyacrylamide and Polymethacrylamide Precursors. *Polymer* **1972**, *13* (10), 462−464.
(48) Yuan, S.; Wang, Z.; Qiao, Z.; Wang, M.; Wang, J.; Wang, S. Improvement of CO2/N2 Separation Characteristics of Polyvinylamine by Modifying with Ethylenediamine. *J. Membr. Sci.* **2011**, *378* (1−2), 425−437.
(49) Chethan, P. D.; Vishalakshi, B. Synthesis of Ethylenediamine Modified Chitosan and Evaluation for Removal of Divalent Metal Ions. *Carbohydr. Polym.* **2013**, *97* (2), 530−536.
(50) Parlar, E. D.; Özten, O.·.; Kızılaslan, A.; Can, M. Synthesis of an Ethylene Diamine Modified Tannin Polymer and Recovery of Gold(III) Ions from Electronic Wastes. *React. Chem. Eng.* **2023**, *8* (5), 1134−1151.
(51) Schelhaas, M.; Waldmann, H. Protecting Group Strategies in Organic Synthesis. *Angew. Chem., Int. Ed.* **1996**, *35* (18), 2056−2083.
(52) Isidro-Llobet, A.; Álvarez, M.; Albericio, F. Amino Acid-Protecting Groups. *Chem. Rev.* **2009**, *109* (6), 2455−2504.
(53) Wu, X.; Hong, R.; Meng, J.; Cheng, R.; Zhu, Z.; Wu, G.; Li, Q.; Wang, C.; Chen, S. Hydrophobic Poly(*Tert* -butyl Acrylate) Photonic Crystals towards Robust Energy-Saving Performance. *Angew. Chem. Int. Ed* **2019**, *58* (38), 13556−13564.
(54) Becker, G.; Wurm, F. R. Functional Biodegradable Polymers *via* Ring-Opening Polymerization of Monomers without Protective Groups. *Chem. Soc. Rev.* **2018**, *47* (20), 7739−7782.

https://doi.org/10.1021/acs.macromol.4c02884
Macromolecules 2025, 58, 5110−5134

(55) Witecka, A.; Schmitt, J.; Courtien, M.; Gérardin, C.; Rydzek, G. Hybrid Mesoporous Silica Materials Templated with Surfactant Polyion Complex (SPIC) Micelles for pH-Triggered Drug Release. *Microporous Mesoporous Mater.* **2024**, *365*, 112913.
(56) Warnant, J.; Reboul, J.; Aqil, A.; Cacciaguerra, T.; Jerome, C.; Gerardin, C. Nanostructured Silica Templated by Double Hydrophilic Block Copolymers with a Comb-like Architecture. *Powder Technol.* **2011**, *208* (2), 461−466.
(57) Panda, S. S.; Hall, C. D.; Oliferenko, A. A.; Katritzky, A. R. Traceless Chemical Ligation from *S* -, *O* -, and *N* -Acyl Isopeptides. *Acc. Chem. Res.* **2014**, *47* (4), 1076−1087.
(58) Raiford, L. C.; Clark, E. P. Behavior Of Mixed O-Acyl-N-Acyl Derivatives In Which The Reacting Groups Are Not On Adjacent Carbon Atoms [1]. *J. Am. Chem. Soc.* **1926**, *48* (2), 483−489.
(59) Watté, J.; Van Gompel, W.; Lommens, P.; De Buysser, K.; Van Driessche, I. Titania Nanocrystal Surface Functionalization through Silane Chemistry for Low Temperature Deposition on Polymers. *ACS Appl. Mater. Interfaces* **2016**, *8* (43), 29759−29769.
(60) Clark, J.; Perrin, D. D. Prediction of the Strengths of Organic Bases. *Q. Rev. Chem. Soc.* **1964**, *18* (3), 295.
(61) Hall, H. K. Correlation of the Base Strengths of Amines [1]. *J. Am. Chem. Soc.* **1957**, *79* (20), 5441−5444.
(62) Bray, C.; Peltier, R.; Kim, H.; Mastrangelo, A.; Perrier, S. Anionic Multiblock Core Cross-Linked Star Copolymers via RAFT Polymerization. *Polym. Chem.* **2017**, *8* (36), 5513−5524.
(63) Lowe, A. B.; McCormick, C. L. Reversible Addition−Fragmentation Chain Transfer (RAFT) Radical Polymerization and the Synthesis of Water-Soluble (Co)Polymers under Homogeneous Conditions in Organic and Aqueous Media. *Prog. Polym. Sci.* **2007**, *32* (3), 283−351.
(64) Phimphachanh, A.; Chamieh, J.; Leclercq, L.; Harrisson, S.; Destarac, M.; Lacroix-Desmazes, P.; Gérardin, C.; In, M.; Cottet, H. Characterization of Diblock Copolymers by Capillary Electrophoresis: From Electrophoretic Mobility Distribution to Distribution of Composition. *Macromolecules* **2020**, *53* (1), 334−345.
(65) Rydzek, G.; Pakdel, A.; Witecka, A.; Awang Shri, D. N.; Gaudière, F.; Nicolosi, V.; Mokarian-Tabari, P.; Schaaf, P.; Boulmedais, F.; Ariga, K. pH-Responsive Saloplastics Based on Weak Polyelectrolytes: From Molecular Processes to Material Scale Properties. *Macromolecules* **2018**, *51* (12), 4424−4434.
(66) Dong, R.; Lindau, M.; Ober, C. K. Dissociation Behavior of Weak Polyelectrolyte Brushes on a Planar Surface. *Langmuir* **2009**, *25* (8), 4774−4779.
(67) Crouzier, T.; Picart, C. Ion Pairing and Hydration in Polyelectrolyte Multilayer Films Containing Polysaccharides. *Biomacromolecules* **2009**, *10* (2), 433−442.
(68) Krężel, A.; Bal, W. A Formula for Correlating p K a Values Determined in D 2 O and H 2 O. *J. Inorg. Biochem.* **2004**, *98* (1), 161−166.
(69) Dewhurst, C. D. Graphical Reduction and Analysis Small-Angle Neutron Scattering Program. *GRASP. J. Appl. Crystallogr.* **2023**, *56* (5), 1595−1609.
(70) Arnold, O.; Bilheux, J. C.; Borreguero, J. M.; Buts, A.; Campbell, S. I.; Chapon, L.; Doucet, M.; Draper, N.; Leal, R. F.; Gigg, M. A.; et al. Mantid - Data Analysis And Visualization Package For Neutron Scattering And μSR$ Experiments. *Nucl. Instrum. Methods Phys. Res. A* **2014**.
(71) Heenan, R. K.; Rogers, S. E.; Turner, D.; Terry, A. E.; Treadgold, J.; King, S. M. Small Angle Neutron Scattering Using Sans2d. *Neutron News* **2011**, *22* (2), 19−21.
(72) Mildner, D. F. R.; Carpenter, J. M. Optimization of the Experimental Resolution for Small-Angle Scattering. *J. Appl. Crystallogr.* **1984**, *17* (4), 249−256.
(73) Pedersen, J. S.; Gerstenberg, M. C. Scattering Form Factor of Block Copolymer Micelles. *Macromolecules* **1996**, *29* (4), 1363−1365.
(74) Mathonnat, M. *Le Rôle de l'eau Dans La Structuration Des Silices Mésoporeuses Par Des Complexes Électrostatiques*, Doctoral dissertation; Université Montpellier, 2017.
(75) Manet, S.; Lecchi, A.; Impéror-Clerc, M.; Zholobenko, V.; Durand, D.; Oliveira, C. L. P.; Pedersen, J. S.; Grillo, I.; Meneau, F.; Rochas, C. Structure of Micelles of a Nonionic Block Copolymer Determined by SANS and SAXS. *J. Phys. Chem. B* **2011**, *115* (39), 11318−11329.
(76) Pedersen, J. S. Form Factors of Block Copolymer Micelles with Spherical, Ellipsoidal and Cylindrical Cores. *J. Appl. Crystallogr.* **2000**, *33* (3), 637−640.
(77) Pedersen, J. S. Structure Factors Effects in Small-Angle Scattering from Block Copolymer Micelles and Star Polymers. *J. Chem. Phys.* **2001**, *114* (6), 2839−2846.
(78) Kinning, D. J.; Thomas, E. L. Hard-Sphere Interactions between Spherical Domains in Diblock Copolymers. *Macromolecules* **1984**, *17* (9), 1712−1718.
(79) Manet, S.; Schmitt, J.; Impéror-Clerc, M.; Zholobenko, V.; Durand, D.; Oliveira, C. L. P.; Pedersen, J. S.; Gervais, C.; Baccile, N.; Babonneau, F.; Grillo, I.; Meneau, F.; Rochas, C. Kinetics of the Formation of 2D-Hexagonal Silica Nanostructured Materials by Nonionic Block Copolymer Templating in Solution. *J. Phys. Chem. B* **2011**, *115* (39), 11330−11344.
(80) Guinier, A.; Fournet, G.; Walker, C. B.; Vineyard, G. H. Small-Angle Scattering of X-Rays. *Phys. Today* **1956**, *9* (8), 38−39.
(81) Hammouda, B. SANS from Homogeneous Polymer Mixtures: A Unified Overview, In *Polymer Characteristics; Advances in Polymer Science*, Springer-Verlag: Berlin/Heidelberg, 1993, Vol. *106*, pp. 87−133. DOI: .
(82) Schweins, R.; Hollmann, J.; Huber, K. Dilute Solution Behaviour of Sodium Polyacrylate Chains in Aqueous NaCl Solutions. *Polymer* **2003**, *44* (23), 7131−7141.
(83) Burchard, W. Static and Dynamic Light Scattering from Branched Polymers and Biopolymers, In *Light Scattering from Polymers; Advances in Polymer Science*, Springer: Berlin Heidelberg, 1983, Vol. *48*, pp. 1−124. DOI: .
(84) Schweins, R.; Lindner, P.; Huber, K. Calcium Induced Shrinking of NaPA Chains: A SANS Investigation of Single Chain Behavior. *Macromolecules* **2003**, *36* (25), 9564−9573.
(85) Tshepelevitsh, S.; Kütt, A.; Lõkov, M.; Kaljurand, I.; Saame, J.; Heering, A.; Plieger, P. G.; Vianello, R.; Leito, I. On the Basicity of Organic Bases in Different Media. *Eur. J. Org. Chem.* **2019**, *2019* (40), 6735−6748.
(86) Tan, W. L.; Tang, L.; Matsidik, R.; Bryant, G.; Martin, T. B.; Sommer, M.; Huang, D. M.; McNeill, C. R. Small-Angle Neutron Scattering of P(NDI2OD-T2) Solutions: Importance of Network Structure for Data Interpretation and Film Morphology. *Macromolecules* **2024**, *57* (2), 691−706.
(87) Schwiertz, D.; Angelina, J.; Zhang, H.; Barz, M. Miktoarm Star-Polypept(o)Ide-Based Polyion Complex Micelles for the Delivery of Large Nucleic Acids. *Biomacromolecules* **2024**, *25*, 6539−6554.
(88) Tonegawa, A.; Tamura, A.; Zhang, S.; Yui, N. Hydrophobicity of Acyl Groups in α-Cyclodextrin-Threaded Polyrotaxanes Dominates the Formation and Stability of Self-Assembled Nanoparticles. *Polymer* **2020**, *200*, 122537.
(89) Bader, R. A.; Silvers, A. L.; Zhang, N. Polysialic Acid-Based Micelles for Encapsulation of Hydrophobic Drugs. *Biomacromolecules* **2011**, *12* (2), 314−320.
(90) Améndola, I. F.; Velasco, M. I.; Acosta, R. H.; Soler Illia, G. J. A. A.; Contreras, C. B. Smart Hybrid Copolymer-Coated Silica Nanosystems with Dual Responsiveness as a Carrier for Positive Charged Molecules. *Eur. Polym. J.* **2024**, *204*, 112717.
(91) Molina, E.; Warnant, J.; Mathonnat, M.; Bathfield, M.; In, M.; Laurencin, D.; Jérôme, C.; Lacroix-Desmazes, P.; Marcotte, N.; Gérardin, C. Drug−Polymer Electrostatic Complexes as New Structuring Agents for the Formation of Drug-Loaded Ordered Mesoporous Silica. *Langmuir* **2015**, *31* (47), 12839−12844.
(92) Yang, Y.; Qi, P.; Ding, Y.; Maitz, M. F.; Yang, Z.; Tu, Q.; Xiong, K.; Leng, Y.; Huang, N. A Biocompatible and Functional Adhesive Amine-Rich Coating Based on Dopamine Polymerization. *J. Mater. Chem. B* **2015**, *3* (1), 72−81.

https://doi.org/10.1021/acs.macromol.4c02884
Macromolecules 2025, 58, 5110−5134

(93) Elhalwagy, M. E.; Elsherbiny, A. S.; Gemeay, A. H. Amine-Rich Polymers for Water Purification Applications. *Mater. Today Chem.* **2023**, *27*, 101344.
(94) Darabi, A.; Jessop, P. G.; Cunningham, M. F. CO_2 -Responsive Polymeric Materials: Synthesis, Self-Assembly, and Functional Applications. *Chem. Soc. Rev.* **2016**, *45* (15), 4391−4436.

https://doi.org/10.1021/acs.macromol.4c02884
Macromolecules 2025, 58, 5110−5134